HEEGAARD DIAGRAMS AND SURGERY DESCRIPTIONS FOR TWISTED FACE-PAIRING 3-MANIFOLDS

J. W. CANNON, W. J. FLOYD, AND W. R. PARRY

Abstract. We give a simple algorithmic construction of a Heegaard diagram for an arbitrary twisted face-pairing 3-manifold. One family of meridian curves in the Heegaard diagram corresponds to the face pairs, and the other family is obtained from the first by a product of powers of Dehn twists. These Dehn twists are along curves which correspond to the edge cycles and the powers are the multipliers. From the Heegaard diagram, one can easily construct a framed link in the 3-sphere such that Dehn surgery on this framed link gives the twisted face-pairing manifold.

1. Introduction

Twisted face-pairing gives a powerful technique for constructing 3-manifolds. Starting with a faceted 3-ball P and an arbitrary orientation-reversing face-pairing ϵ on P, one constructs a faceted 3-ball Q and an orientation-reversing face-pairing δ on Q such that the quotient Q/δ is a manifold. Here Q is obtained from P by subdividing the edges according to a function which assigns a positive integer (called a multiplier) to each edge cycle, and δ is obtained from ϵ by precomposing each face-pairing map with a twist. Which direction to twist depends on choosing an orientation of P. Hence for a given faceted 3-ball P, orientation-reversing face-pairing ϵ, and multiplier function, one obtains two twisted face-pairing manifolds $M = Q/\delta$ and $M^* = Q/\delta^*$ (one for each orientation of P).

In [1] and [2] we introduced twisted face-pairing 3-manifolds and developed their first properties. A surprising result in [2] is the duality theorem that says that, if P is a regular faceted 3-ball, then M and M^* are homeomorphic in a way that makes their cell structures dual to each other. This duality is instrumental in [3], where we investigated a special subset of these manifolds, the ample twisted face-pairing manifolds. We showed that the fundamental group of every ample twisted face-pairing manifold is Gromov hyperbolic with space at infinity a 2-sphere.

In this paper we connect the twisted face-pairing construction with two standard 3-manifold constructions. Starting with a faceted 3-ball P with $2g$ faces and an orientation-reversing face-pairing ϵ on P, we construct a closed surface S of genus g and two families γ and β of pairwise disjoint simple closed curves on S. The elements of γ correspond to the face pairs and the elements of β correspond to the edge cycles of ϵ. Given a choice of multipliers for the edge cycles, we then give a Heegaard diagram for the resulting twisted face-pairing 3-manifold. The surface S is the Heegaard surface, and the family γ is one of the two families of meridian

Date: July 24, 2001.
1991 *Mathematics Subject Classification.* 57N10.
Key words and phrases. 3-manifold constructions, Dehn surgery, Heegaard diagrams.
This research was supported in part by NSF research grants.

curves. The other family is obtained from γ by a product of powers of Dehn twists along elements of β; the powers of the Dehn twists are the multipliers. From the Heegaard diagram, one can easily construct a framed link in the 3-sphere such that Dehn surgery on this framed link gives the twisted face-pairing manifold. The components of the framed link fall naturally into two families; each curve in one family corresponds to a face pair and has framing 0, and each curve in the other family corresponds to an edge cycle and has framing the sum of the reciprocal of its multiplier and the blackboard framing of a certain projection of the curve. These results are very useful for understanding both specific face-pairing manifolds and entire classes of examples. While we defer most illustrations of these results to a later paper [4], we give several examples here to illustrate how to easily use these results to give familiar names to some twisted face-pairing 3-manifolds.

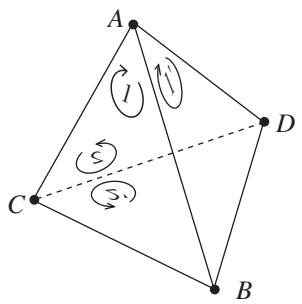

FIGURE 1. The complex P.

We give a preliminary example to illustrate the twisted face-pairing construction. Let P be the tetrahedron with vertices A, B, C, and D, as shown in Figure 1. Consider the face-pairing $\epsilon = \{\epsilon_1, \epsilon_2\}$ on P with map ϵ_1 which takes triangle ABC to triangle ABD fixing the edge AB and map ϵ_2 which takes triangle ACD to BCD fixing the edge CD. This example was considered briefly in [1] and in more detail in [2, Example 3.2]. The edge cycles are the equivalence classes of the edges of P under the face-pairing maps. The three edge cycles are $\{AB\}$, $\{BC, BD, AD, AC\}$, and $\{CD\}$; the associated diagrams of face-pairing maps are shown below.

$$AB \xrightarrow{\epsilon_1} AB$$

$$BC \xrightarrow{\epsilon_1} BD \xrightarrow{\epsilon_2^{-1}} AD \xrightarrow{\epsilon_1^{-1}} AC \xrightarrow{\epsilon_2} BC$$

$$CD \xrightarrow{\epsilon_2} CD$$

To construct a twisted face-pairing manifold from P, for each edge cycle $[e]$ we choose a positive integer $\mathrm{mul}([e])$ called the multiplier of $[e]$. Let Q be the subdivision of P obtained by subdividing each edge e of P into $\#([e]) \cdot \mathrm{mul}([e])$ subedges. The face-pairing maps ϵ_1 and ϵ_2 naturally give face-pairing maps on the faces of Q. Choose an orientation of ∂Q, and define the twisted face-pairing δ on Q by precomposing each ϵ_i with an orientation-preserving homeomorphism of its domain which takes each vertex to the vertex that follows it in the induced orientation on the boundary. By the fundamental theorem of twisted face-pairings (see [1] or [2]), the quotient Q/δ is a closed 3-manifold.

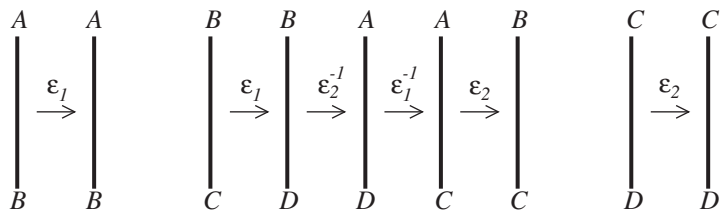

FIGURE 2. The edge diagrams.

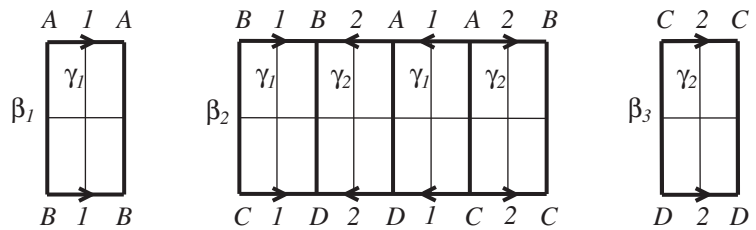

FIGURE 3. The rectangles that correspond to the edge diagrams.

To construct a Heegaard diagram and framed link for the twisted face-pairing manifold Q/δ, we first schematically indicate edge diagrams as shown in Figure 2. We then make rectangles out of the edge diagrams in Figure 3, and add thin horizontal and vertical line segments through the midpoints of each of the subrectangles of the rectangles. We identify the boundary edges of the rectangles in pairs preserving the vertex labels (and, for horizontal edges, the order) to get a quotient surface S of genus two. The image in S of the thin vertical arcs is a union of two disjoint simple closed curves γ_1 and γ_2, which correspond to the two face pairs. The image in S of the thin horizontal arcs is a union of three pairwise disjoint simple closed curves β_1, β_2, and β_3, which correspond to the three edge cycles. Figure 4 shows S as the quotient of the union of two annuli, and Figure 5 shows the curve families $\{\gamma_1, \gamma_2\}$ and $\{\beta_1, \beta_2, \beta_3\}$ on S. For $i \in \{1, 2, 3\}$, let m_i be the multiplier of the edge cycle corresponding to β_i and let τ_i be one of the two Dehn twists along β_i. We choose τ_1, τ_2, and τ_3 so that they are oriented consistently. Let $\tau = \tau_1^{m_1} \circ \tau_2^{m_2} \circ \tau_3^{m_3}$. It follows from Theorem 6.1.1 that S and $\{\gamma_1, \gamma_2\}$ and $\{\tau(\gamma_1), \tau(\gamma_2)\}$ form a Heegaard diagram for the twisted face-pairing manifold Q/δ. From the Heegaard diagram, one can use standard techniques to give a framed surgery description for Q/δ. An algorithmic description for this is given in Theorem 6.1.2. In the present example, the surgery description is shown in Figure 6 together with a modification of the 1-skeleton of the tetrahedron P. There are two curves with framing 0, corresponding to the two pairs of faces. The other three curves correspond to the edge cycles and have framings the reciprocals of the multipliers.

We now describe our Heegaard diagram construction in greater detail. We use the notation and terminology of [2]. Let P be a faceted 3-ball, let ϵ be an orientation-reversing face-pairing on P and let mul be a multiplier function for ϵ. (As in [2], we for now assume that P is a regular CW complex. We drop the regularity assumption in Section 2.) Let Q be the twisted face-pairing subdivision of P, let δ be the twisted face-pairing on Q, and let M be the associated twisted

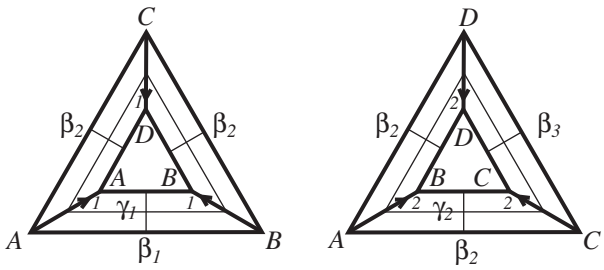

FIGURE 4. Another view of the surface S.

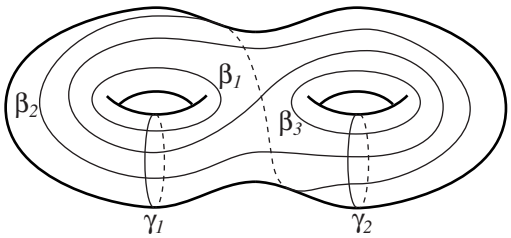

FIGURE 5. The curve families $\{\gamma_1, \gamma_2\}$ and $\{\beta_1, \beta_2, \beta_3\}$ on the surface S.

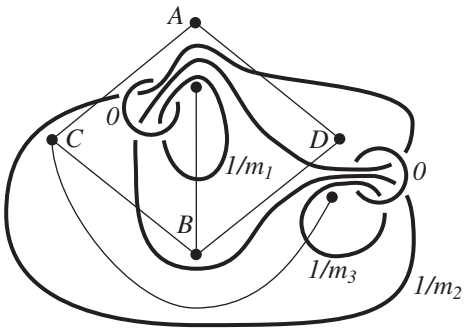

FIGURE 6. The surgery description.

face-pairing manifold. We next construct a closed surface S with the structure of a cell complex. For this we first construct a cell complex X cellularly homeomorphic to the 1-skeleton of Q. Suppose given two paired faces f and f^{-1} of Q. We choose one of these faces, say f, and we construct $\partial f \times [0,1]$. We view the interval $[0,1]$ as a 1-cell, and we view $\partial f \times [0,1]$ as a 2-complex with the product cell structure. For every $x \in \partial f$ we identify $(x,0) \in \partial f \times [0,1]$ with the point in X corresponding to x and we identify $(x,1) \in \partial f \times [0,1]$ with the point in X corresponding to $\delta_f(x) \in \partial f^{-1}$. Doing this for every pair of faces of Q yields a cell complex Y on a closed surface. We define S to be the first dual cap subdivision of Y; because every face of Y is a quadrilateral, this simply means that to obtain S from Y we subdivide every face of Y into four quadrilaterals in the straightforward way. We say that an edge of S is vertical if it is either contained in X or is disjoint from

X. We say that an edge of S is diagonal if it is not vertical. The union of the vertical edges of S which are not edges of Y is a family of simple closed curves in S. Likewise the union of the diagonal edges of S which are not edges of Y is a family of simple closed curves in S. Theorem 4.3.1 states that the surface S and these two families of curves form a Heegaard diagram for M.

In this paragraph we indicate how to associate to a given edge cycle E of ϵ a closed subspace of S. To simplify this discussion we assume that E contains three edges and that $\mathrm{mul}(E) = 2$. When constructing Q from P, every edge of E is subdivided into $2 \cdot 3 = 6$ subedges. So corresponding to the three edges of E, the complex S contains three 1-complexes, each of them homeomorphic to an interval and the union of 12 vertical edges of S. These three 1-complexes and part of S are shown in Figure 7; the three 1-complexes are drawn as four thick vertical line segments with the left one to be identified with the right one. We refer to the closed subspace C of S shown in Figure 7 as an edge cycle cylinder or simply as a cylinder. In Figure 7, vertical edges of S are drawn vertically and diagonal edges of S are drawn diagonally. Some arcs in Figure 7 are dashed because they are not contained in the 1-skeleton of S. The thick edges in Figure 7 are the edges of Y in C. (It is interesting to note that these thick edges essentially give the diagram in Figure 11 of [2].) Note that the edge cycle cylinder C need not be a closed annulus, although C is the closure of an open annulus. (Identifications of boundary points are possible.) We choose these edge cycle cylinders so that their union is S and the cylinders of distinct ϵ-edge cycles have disjoint interiors.

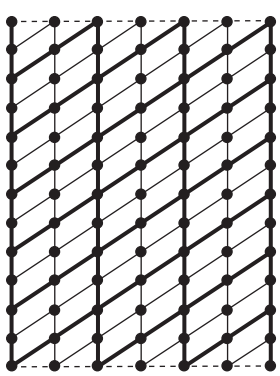

FIGURE 7. The cylinder C corresponding to the edge cycle E.

We define the circumference of an edge cycle cylinder to be the number of edges in its edge cycle. We define the height of an edge cycle cylinder to be the number of edges in its edge cycle times the multiplier of its edge cycle. The edge cycle cylinder C in Figure 7 contains three arcs ρ_1, ρ_2, ρ_3 whose endpoints lie on dashed arcs such that each of ρ_1, ρ_2, ρ_3 is a union of thin vertical edges. Likewise C contains three arcs σ_1, σ_2, σ_3 such that each of σ_1, σ_2, σ_3 is a union of thin diagonal edges and the endpoints of σ_i equal the endpoints of ρ_i for every $i \in \{1, 2, 3\}$. Because the height of C equals 2 times the circumference of C, it follows that σ_1, σ_2, σ_3 can be realized as the images of ρ_1, ρ_2, ρ_3 under the second power of a Dehn twist along a waist of C. This observation and the previous paragraphs essentially give the following. Let $\alpha_1, \ldots, \alpha_n$ be the simple closed curves in S which are unions of vertical edges of S but not Y. Let $E_1, \ldots, E_m$ be the edge cycles of ϵ. For every $i \in \{1, \ldots, m\}$

construct a waist β_i in the edge cycle cylinder of E_i so that $\beta_1, \ldots, \beta_m$ are pairwise disjoint simple closed curves in S. For every $i \in \{1, \ldots, m\}$ let τ_i be one of the two Dehn twists on S along β_i, chosen so that the directions in which we twist are consistent. Set $\tau^{\mathrm{mul}} = \tau_1^{\mathrm{mul}(E_1)} \circ \cdots \circ \tau_m^{\mathrm{mul}(E_m)}$. Then S and $\alpha_1, \ldots, \alpha_n$ and $\tau^{\mathrm{mul}}(\alpha_1), \ldots, \tau^{\mathrm{mul}}(\alpha_n)$ form a Heegaard diagram for M. The last statement is the content of Theorem 6.1.1.

The result of the previous paragraph leads to a link L in S^3 such that L has components $\gamma_1, \ldots, \gamma_n$ and $\delta_1, \ldots, \delta_m$, where $\gamma_1, \ldots, \gamma_n$ correspond to $\alpha_1, \ldots, \alpha_n$ and $\delta_1, \ldots, \delta_m$ correspond to $\beta_1, \ldots, \beta_m$. We define a framing of L so that $\gamma_1, \ldots, \gamma_n$ have framing 0 and for every $i \in \{1, \ldots, m\}$ δ_i has framing $\mathrm{mul}(E_i)^{-1}$ plus the blackboard framing of δ_i relative to a certain projection. Then the manifold obtained by Dehn surgery on L is homeomorphic to M. The last statement is the content of Theorem 6.1.2. At last we see that multipliers of edge cycles are essentially inverses of framings of link components. In Section 6.2 we make the construction of L algorithmic and simple using what we call the corridor construction.

Although we know of no nice characterization of twisted face-pairing 3-manifolds, Theorem 5.3.1 gives such a characterization of their Heegaard diagrams. Theorem 5.3.1 and results leading to it give the following statements. Every irreducible Heegaard diagram for an orientable closed 3-manifold M gives rise to a faceted 3-ball P with orientation-reversing face-pairing ϵ (in essentially two ways – one for each family of meridian curves) such that P/ϵ is homeomorphic to M. Every irreducible Heegaard diagram can be decomposed into cylinders, which we call Heegaard cylinders, essentially just as our above Heegaard diagrams of twisted face-pairing manifolds are decomposed into edge cycle cylinders. In general heights of Heegaard cylinders are not multiples of their circumferences. A given irreducible Heegaard diagram is the Heegaard diagram, as constructed above, of a twisted face-pairing manifold if and only if the height of each of its Heegaard cylinders is a multiple of its circumference. Furthermore, if the height of every Heegaard cylinder is a multiple of its circumference, then the face-pairing ϵ constructed from the given Heegaard diagram is a twisted face-pairing.

Thus far we have discussed the construction of Heegaard diagrams for twisted face-pairing manifolds and the construction of face-pairings from irreducible Heegaard diagrams. In Theorem 4.2.1 we more generally construct (irreducible) Heegaard diagrams for manifolds of the form P/ϵ, where P is a faceted 3-ball with orientation-reversing face-pairing ϵ and the cell complex P/ϵ is a manifold with one vertex. In Theorem 5.3.1 we construct for every irreducible Heegaard diagram for a 3-manifold M a faceted 3-ball P with orientation-reversing face-pairing ϵ (in essentially two ways – one for each family of meridian curves) such that P/ϵ is a cell complex with one vertex and P/ϵ is homeomorphic to M. These two constructions are essentially inverse to each other.

The above statements that every irreducible Heegaard diagram gives rise to a faceted 3-ball require a more general definition of faceted 3-ball than the one given in [2]. In [2] faceted 3-balls are regular, that is, for every open cell of a faceted 3-ball the prescribed homeomorphism of an open Euclidean ball to that cell extends to a homeomorphism of the closed Euclidean ball to the closed cell. On the other hand, the cellulation of the boundary of a 3-ball which arises from a Heegaard diagram has paired faces but otherwise is arbitrary. So we now define a faceted 3-ball P to be an oriented CW complex such that P is a closed 3-ball, the interior of P is the unique

open 3-cell of P, and the cell structure of ∂P does not consist of just one 0-cell and one 2-cell. This generalization presents troublesome minor technical difficulties but no essential difficulties. In particular, all the results of [1] and [2] hold for these more general faceted 3-balls. Section 2 deals with this generalization. Except when the old definition is explicitly discussed, we henceforth in this paper use the new definition of faceted 3-ball. We know of no reducible twisted face-pairing manifold which arises from a regular faceted 3-ball; the old twisted face-pairing manifolds all seem to be irreducible. On the other hand the new twisted face-pairing manifolds are often reducible. See the related Examples 2.1, 4.3.2 and 7.1 and the related Examples 2.3, and 6.2.1.

Our construction of Heegaard diagrams from face-pairings uses a subdivision of cell complexes which we call dual cap subdivision. We define and discuss dual cap subdivision in Section 3. The term "dual" is motivated by the notion of dual cell complex, and the term "cap" is motivated by its association with intersection. Intuitively, the dual cap subdivision of a cell complex is gotten by "intersecting" the complex with its "dual complex". Dual cap subdivision is coarser than barycentric subdivision, and it is well suited to the constructions at hand. Heegaard decompositions of 3-manifolds are usually constructed by triangulating the manifolds and working with their second barycentric subdivisions. Instead of using barycentric subdivision, we use dual cap subdivision, and we obtain the following. Earlier in the introduction we construct a surface S with a cell structure. We show that S is cellularly homeomorphic to a subcomplex of the second dual cap subdivision of the manifold M, where this subcomplex corresponds to the usual Heegaard surface gotten by using a triangulation and barycentric subdivision.

In Section 7 we use the corridor construction of Section 6.2 to construct links in S^3 for three different model face-pairings. Simplifying these links using isotopies and Kirby calculus, we are able to identify the corresponding twisted face-pairing manifolds. In Example 7.1 we obtain the connected sum of the lens space $L(p, 1)$ and the lens space $L(r, 1)$ as a twisted face-pairing manifold, where p and r are positive integers. In Example 7.2 we obtain all integer Dehn surgeries on the figure eight knot as twisted face-pairing manifolds. In Example 7.3 we obtain the Heisenberg manifold, the prototype of Nil geometry. In Example 6.2.1 we obtain $S^2 \times S^1$.

Which orientable closed 3-manifolds are twisted face-pairing manifolds? As far as we know they all are, although that seems rather unlikely. An interesting problem is to determine whether the 3-torus is a twisted face-pairing manifold; we do not know whether it is or not. In a later paper [4] we present a survey of twisted face-pairing 3-manifolds which indicates the scope of the set of twisted face-pairing manifolds. Here are some of the results in [4]. We show how to obtain every lens space as a twisted face-pairing manifold. We consider the faceted 3-balls for which every face is a digon, and we show that the twisted face-pairing manifolds obtained from these faceted 3-balls are Seifert fibered manifolds. We show how to obtain most Seifert fibered manifolds. We show that if M_1 and M_2 are twisted face-pairing manifolds, then so is the connected sum of M_1 and M_2.

2. Generalizing the construction

Our twisted face-pairing construction begins with a faceted 3-ball. In Section 2 of [2] we define a faceted 3-ball P to be an oriented regular CW complex such that P is a closed 3-ball and P has a single 3-cell. In this section we generalize our

twisted face-pairing construction by generalizing the notion of faceted 3-ball. This generalization gives us more freedom in constructing twisted face-pairing manifolds, and it is natural in the context of Theorem 5.3.1.

We take cells of cell complexes to be closed unless explicitly stated otherwise.

We now define a faceted 3-ball P to be an oriented CW complex such that P is a closed 3-ball, the interior of P is the unique open 3-cell of P, and the cell structure of ∂P does not consist of just one 0-cell and one 2-cell. Suppose that P is an oriented CW complex such that P is a closed 3-ball and the interior of P is the unique open 3-cell of P. The condition that the cell structure of ∂P does not consist of just one 0-cell and one 2-cell is equivalent to the following useful condition. For every 2-cell f of P there exists a CW complex F such that F is a closed disk, the interior of F is the unique open 2-cell of F, and there exists a continuous cellular map $\varphi\colon F \to f$ such that the restriction of φ to every open cell of F is a homeomorphism. So f is gotten from F by identifying some vertices and identifying some pairs of edges. The number of vertices and edges in F is uniquely determined. This definition of faceted 3-ball allows for faces such as those in Figure 8, which were not allowed before; part a) of Figure 8 shows a quadrilateral and part b) of Figure 8 shows a pentagon. To overcome difficulties presented by faces such as those in Figure 8, the next thing that we do is subdivide P.

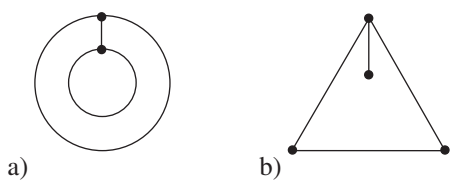

FIGURE 8. Faces now allowed in a faceted 3-ball.

In this paragraph we construct a subdivision P_s of a given faceted 3-ball P. The idea is to not subdivide the 3-cell of P and to construct what might be called the barycentric subdivision of ∂P. The vertices of P_s are the vertices of P together with a barycenter for every edge of P and a barycenter for every face of P. Every face of P_s is a triangle contained in ∂P. If t is one of these triangles, then one vertex of t is a vertex of P, one vertex of t is a barycenter of an edge of P, and one vertex of t is a barycenter of a face of P. The only 3-cell of P_s is the 3-cell of P. This determines P_s. Given a face f of P, we let f_s denote the subcomplex of P_s which consists of the cells of P_s contained in f. Figure 9 shows f_s for each of the faces f in Figure 8.

In this paragraph we make two related definitions. Let P be a faceted 3-ball, and let f be a face of P. We define a **corner** of f at a vertex v of f to be a subcomplex of f_s consisting of the union of two faces of f_s which both contain an edge e such that e contains v and the barycenter of f. We define an **edge cone** of f at an edge e of f to be a subcomplex of f_s consisting of the union of two faces of f_s which both contain an edge e' such that e' contains the barycenter of f and the barycenter of e.

Now a face-pairing ϵ on a given faceted 3-ball P consists of the following. First, the faces of P are paired: for every face f of P there exists a face $f^{-1} \neq f$ of P such that $(f^{-1})^{-1} = f$. Second, the faces of P_s are paired: for every face t of P_s contained in a face f of P there exists a face t^{-1} of P_s with $t^{-1} \subseteq f^{-1}$ such that $(t^{-1})^{-1} = t$.

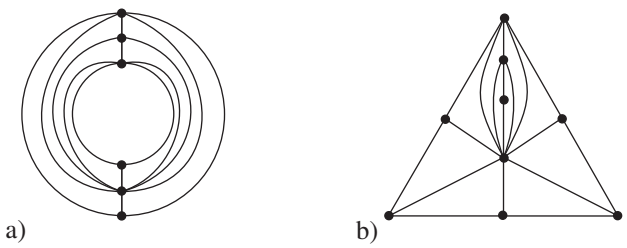

FIGURE 9. The subdivisions of the faces in Figure 8.

Third, for every face t of P_s there exists a cellular homeomorphism $\epsilon_t\colon t \to t^{-1}$ called a partial face-pairing map such that $\epsilon_{t^{-1}} = \epsilon_t^{-1}$. We require that ϵ_t maps the vertex of P in t to the vertex of P in t^{-1}, that ϵ_t maps the edge barycenter in t to the edge barycenter in t^{-1}, and that ϵ_t maps the face barycenter in t to the face barycenter in t^{-1}. Furthermore, the faces of P_s are paired and the partial face-pairing maps are defined so that if t and t' are faces of P_s contained in some face f of P and if e is an edge of $t \cap t'$ which contains the barycenter of f, then $\epsilon_t|_e = \epsilon_{t'}|_e$. For every face f of P we set $\epsilon_f = \{\epsilon_t\colon t \text{ is a face of } f_s\}$, and we refer to ϵ_f as a multivalued face-pairing map from f to f^{-1}. We set $\epsilon = \{\epsilon_f\colon f \text{ is a face of } P\}$. In a straightforward way we obtain a quotient space P_s/ϵ consisting of orbits of points of P_s under ϵ. Finally, we impose a face-pairing compatibility condition on ϵ just as in Section 2 of [2] to ensure that P_s/ϵ is a cell complex. It is easy to see that the cell structure of P induces a cell structure on P_s/ϵ, and it is this cell structure that we put on P_s/ϵ, not the cell structure induced from P_s. We usually write P/ϵ instead of P_s/ϵ. We usually want ϵ to be orientation reversing, which means that every partial face-pairing map of ϵ reverses orientation.

Let P be a faceted 3-ball, let f be a face of P, and suppose that ϵ is an orientation-reversing face-pairing on P. Then the multivalued face-pairing map ϵ_f determines a function from the set of corners of f to the set of corners of f^{-1} in a straightforward way. The image of one corner of f under this function determines the image of every corner of f under this function. The action of ϵ on the set of corners of the faces of P determines P_s/ϵ up to homeomorphism. Thus for our purposes to define the multivalued face-pairing map ϵ_f of a face f of P, it suffices to give a corner c of f and the corner of f^{-1} to which ϵ_f maps c.

Let ϵ be an orientation-reversing face-pairing on a faceted 3-ball P. Essentially as in Section 2 of [2], ϵ partitions the edges of P into edge cycles. (We consider the edges of P, not the edges of P_s.) To every edge cycle E of ϵ we associate a length ℓ_E and a multiplier m_E as before. The function $\mathrm{mul}\colon \{\text{edge cycles}\} \to \mathbf{N}$ defined by $E \mapsto m_E$ is called the multiplier function. We obtain a twisted face-pairing subdivision Q from P just as before: if e is an edge of P and if E is the edge cycle of ϵ containing e, then we subdivide e into $\ell_E m_E$ subedges. As before, we subdivide in an ϵ-invariant way. We likewise construct Q_s in an ϵ-invariant way. It follows that ϵ naturally determines a face-pairing on Q, which we continue to call ϵ, abusing notation more than before.

We consider face twists in this paragraph. In the present setting a face twist is not a single cellular homeomorphism, but instead a collection of cellular homeomorphisms. For this, we maintain the situation of the previous paragraph. Let f be a face of Q. Let t be a face of f_s. The orientation of f determines a cyclic order

on the faces of f_s. Let t' be the second face of f_s which follows t relative to this cyclic order. Let τ_t be an orientation-preserving cellular homeomorphism from t to t' such that τ_t fixes the barycenter of f. We call $\tau_f = \{\tau_t\colon\ t \text{ is a face of } f_s\}$ the face twist of f. We assume that if t_1 and t_2 are faces of f_s and if e is an edge of $t_1 \cap t_2$ which contains the barycenter of f, then $\tau_{t_1}|_e = \tau_{t_2}|_e$. We also assume that our face twists are defined ϵ-invariantly: for each face f of Q and each face t of f_s, we have $\tau_{t^{-1}} = \epsilon_{t''} \circ \tau_{t''}^{-1} \circ \epsilon_{t^{-1}}$, where t'' is the second face of f_s which precedes t. We furthermore impose a compatibility condition on our face twists in the next paragraph.

Now we are prepared to define a twisted face-pairing δ on Q. We pair the faces of Q just as the faces of P are paired. The pairing of the faces of P_s likewise induces a pairing of the faces of Q_s. For every face f of Q and every face t of f_s, we set $\delta_t = \epsilon_{t'} \circ \tau_t$, where t' is the second face of f_s which follows t. For every face f of Q we set $\delta_f = \{\delta_t\colon\ t \text{ is a face of } f_s\}$, and we set $\delta = \{\delta_f\colon\ f \text{ is a face of } Q\}$. We assume that the maps τ_t are defined so that δ satisfies the face-pairing compatibility condition. Then δ is a face-pairing on Q called the twisted face-pairing.

Finally, we define $M = M(\epsilon, \mathrm{mul})$ to be the quotient space Q_s/δ. We emphasize that for a cell structure on M we take the cell structure induced from Q, not the cell structure induced from Q_s. The cell complex M is determined up to homeomorphism by the function mul and the action of ϵ on the corners of the faces of P.

Let P be a faceted 3-ball, let ϵ be an orientation-reversing face-pairing on P, and let mul be a multiplier function for ϵ. The results of [2] all hold in this more general setting. So M is an orientable closed 3-dimensional manifold with one vertex. The dual of the link of that vertex is isomorphic to ∂Q^* as oriented 2-complexes, where Q^* is a faceted 3-ball gotten from Q by reversing orientation. We label and direct the faces and edges of Q and Q^* as before. We again obtain a duality between M and M^*. Et cetera.

The proofs in [2] are valid in the present more general setting with only straightforward minor technical modifications and the following. To obtain a duality between M and M^* in [2], we construct a dual cap subdivision Q_σ of Q. We let $C_1, \ldots, C_k$ be the 3-cells of Q_σ, and for every $i \in \{1, \ldots, k\}$ we let A_i be a cell complex isomorphic to C_i so that $A_1, \ldots, A_k$ are pairwise disjoint. Then the vertices of Q can be enumerated as $x_1, \ldots, x_k$ so that C_i is the unique 3-cell of Q_σ which contains x_i for $i \in \{1, \ldots, k\}$. If x_i has valence v_i, then A_i is an alternating suspension on a $2v_i$-gon for $i \in \{1, \ldots, k\}$. In the present setting the 3-cells of Q_σ need not be alternating suspensions; they are quotients of alternating suspensions. See Section 3.2 for a discussion of the 3-cells of Q_σ. So in the present setting we let $x_1, \ldots, x_k$ be the vertices of Q with valences $v_1, \ldots, v_k$, and for $i \in \{1, \ldots, k\}$ we simply define A_i to be an alternating suspension on a $2v_i$-gon. As in [2] the twisted face-pairing δ on Q induces in a straightforward way what might be called a face-pairing on the disjoint union of $A_1, \ldots, A_k$. At this point we proceed as in [2].

We conclude this section with two simple examples to illustrate some of the new phenomena which occur for our more general faceted 3-balls.

Example 2.1. *Let the model faceted 3-ball P be as indicated in Figure 10 with two monogons and two quadrilaterals, the outer monogon being at infinity. The inner monogon has label 1 and is directed outward. The outer monogon has label 1 and is*

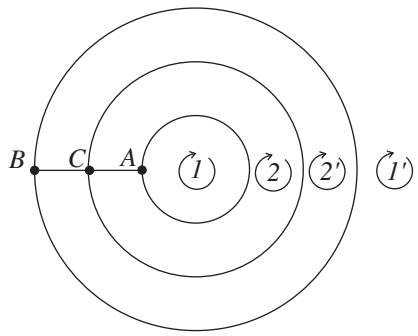

FIGURE 10. The complex P for Example 2.1.

directed inward. The inner quadrilateral has label 2 and is directed outward. The outer quadrilateral has label 2 and is directed inward. As usual for faces in figures, all four faces are oriented clockwise. We construct an orientation-reversing face-pairing ϵ on P as follows. Multivalued face-pairing map ϵ_1 maps the inner monogon to the outer monogon, there being essentially only one way to do this. Multivalued face-pairing map ϵ_2 maps the inner quadrilateral to the outer quadrilateral fixing their common edge. Set $\epsilon = \{\epsilon_1^{\pm 1}, \epsilon_2^{\pm 1}\}$.

We might view this face-pairing as follows. Construct a monogon in the open northern hemisphere of the 2-sphere S^2, put a vertex on the equator of S^2 and join the two vertices with an edge. Now vertically project this cellular decomposition of the northern hemisphere into the southern hemisphere.

The edge cycles for ϵ have the following diagrams.

$$CC \xrightarrow{\epsilon_2} CC \qquad AC \xrightarrow{\epsilon_2} BC \xrightarrow{\epsilon_2^{-1}} AC \qquad BB \xrightarrow{\epsilon_2^{-1}} AA \xrightarrow{\epsilon_1} BB \tag{2.2}$$

For now let the first edge cycle have multiplier 4, let the second have multiplier 1 and let the third have multiplier 1.

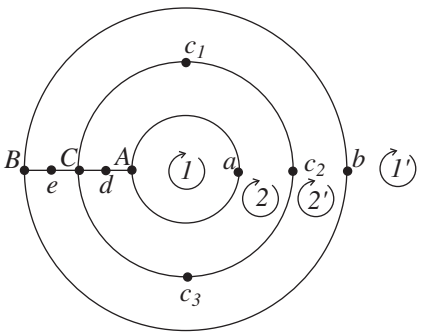

FIGURE 11. The complex Q for Example 2.1.

Figure 11 shows the faceted 3-ball Q. We label the new vertices of Q arbitrarily. Figure 12 shows the link of the vertex of M, with conventions as in [2]*. Figure 13 shows the faceted 3-ball Q^* dual to Q with its edge labels and directions. It is easy to see that ∂Q^* is dual to the link of the vertex of M. We obtain a presentation for the fundamental group G of M as follows. Corresponding to the face labels 1*

and 2 we have generators x_1 and x_2. The boundary of the face of Q^* labeled 1 and directed outward gives the relator $x_1x_2^{-1}$. The boundary of the face of Q^* labeled 2 and directed outward gives the relator $x_2^5x_1^{-1}$. So

$$G \cong \langle x_1, x_2 \colon\ x_1x_2^{-1}, x_2^5x_1^{-1}\rangle \cong \mathbf{Z}/4\mathbf{Z}.$$

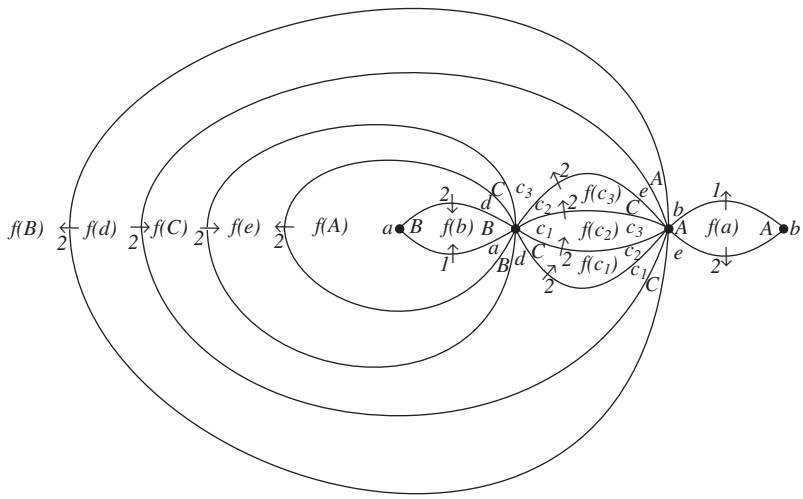

FIGURE 12. The link of the vertex of M.

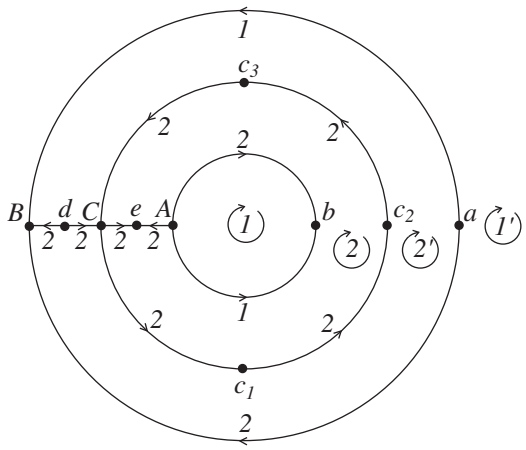

FIGURE 13. The complex Q^* with edge labels and directions.

We will see in Example 7.1 that M is the lens space $L(4,1)$. In general, if the first edge cycle of ϵ has multiplier p, if the second edge cycle of ϵ has multiplier q, and if the third edge cycle of ϵ has multiplier r, then we will see in Example 7.1 that M is the connected sum of the lens space $L(p,1)$ and the lens space $L(r,1)$ (and so in particular M does not depend on q).

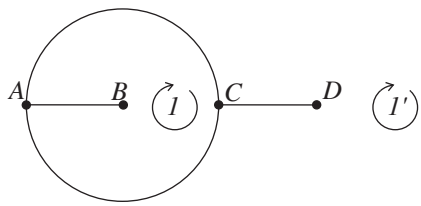

FIGURE 14. The complex P for Example 2.3.

Example 2.3. *Let the model faceted 3-ball P be as in Figure 14 with two quadrilaterals, the outer quadrilateral being at infinity. The inner quadrilateral has label 1 and is directed outward. The outer quadrilateral has label 1 and is directed inward. The orientation-reversing multivalued face-pairing map ϵ_1 maps the inner quadrilateral to the outer quadrilateral taking vertex C to vertex D. Set $\epsilon = \{\epsilon_1^{\pm 1}\}$.*

The vertices A and C of P are joined by two edges. We use the subscripts u and d for up and down to distinguish them. So AC_u is the upper edge joining A and C, and AC_d is the lower edge joining A and C. The face-pairing ϵ has only one edge cycle, and this edge cycle has the following diagram.

$$AC_u \xrightarrow{\epsilon_1} CD \xrightarrow{\epsilon_1^{-1}} AC_d \xrightarrow{\epsilon_1^{-1}} BA \xrightarrow{\epsilon_1} AC_u$$

For simplicity let this edge cycle have multiplier 1.

Figure 15 shows the faceted 3-ball Q. We label the new vertices of Q arbitrarily. Figure 16 shows the link of the vertex of M. Figure 17 shows the faceted 3-ball Q^* dual to Q with its edge labels and directions. It is easy to see that ∂Q^* is dual to the link of the vertex of M. We obtain a presentation for the fundamental group G of M as follows. Corresponding to the face label 1 we have a generator x_1. The boundary of the face of Q^* labeled 1 and directed outward gives the trivial relator. So G has one generator and no relators, that is, $G \cong \mathbf{Z}$.

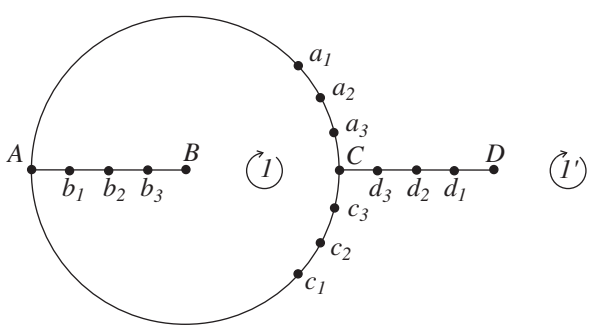

FIGURE 15. The complex Q for Example 2.3.

We will see in Example 6.2.1 that M is homeomorphic to $S^2 \times S^1$ for every choice of multiplier for the edge cycle of ϵ.

3. DUAL CAP SUBDIVISION

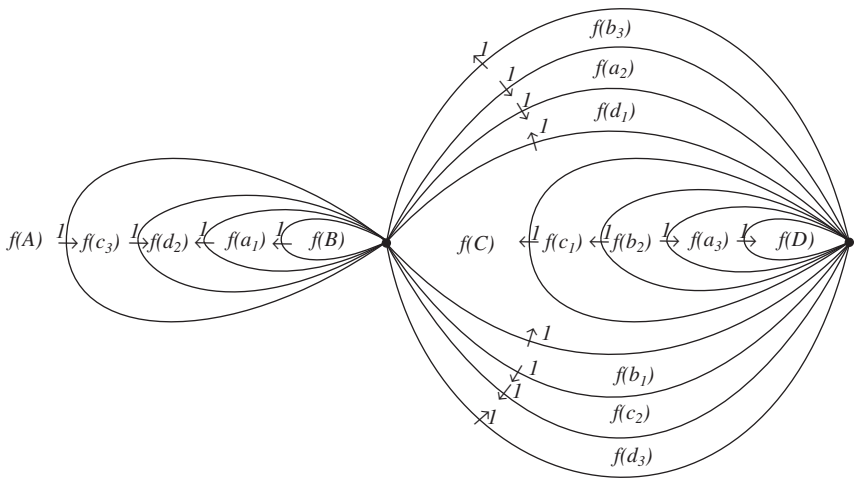

FIGURE 16. The link of the vertex of M.

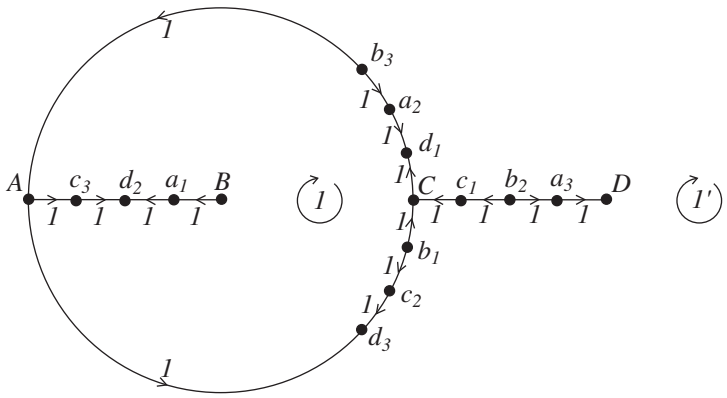

FIGURE 17. The complex Q^* with edge labels and directions.

3.1. **Definition.** Recall that we discussed dual cap subdivision in Section 4 of [2]. Of course, there our faceted 3-balls are regular. We generalize to our present cell complexes in a straightforward way.

Let P be a faceted 3-ball. We construct a dual cap subdivision P_σ of P as follows. The vertices of P_σ consist of the vertices of the subdivision P_s defined in Section 2 together with a barycenter for the 3-cell of P. We next describe the edges of P_σ.

The edges of ∂P_σ consist of the edges of P_s which do not join the barycenter of a face of P and a vertex of that face. For every face of P, the subdivision P_σ also contains an edge joining the barycenter of that face and the barycenter of the 3-cell of P. These are all the edges of P_σ.

Having described the edges of P_σ, the structure of ∂P_σ is determined. The faces of ∂P_σ are in bijective correspondence with the corners of the faces of P. Every face of ∂P_σ is a quadrilateral whose underlying space equals the underlying space of a corner c at a vertex v of a face f of P. Of course, this quadrilateral contains the barycenter a of f. The first diagram in Figure 18 shows this quadrilateral if c

has three vertices and f is a monogon. The second diagram in Figure 18 shows this quadrilateral if c has three vertices and f is not a monogon. The third diagram in Figure 18 shows this quadrilateral if c has four vertices. In the first two diagrams b is the barycenter of the edge of f that contains v, and in the third diagram b_1 and b_2 are the barycenters of the two edges of f that contain v.

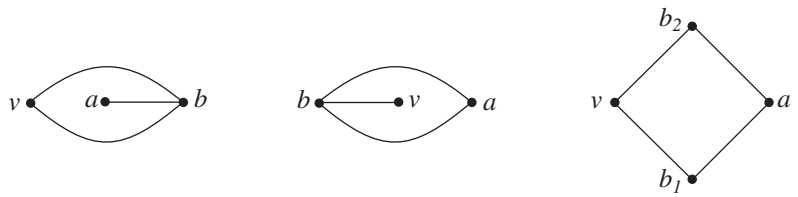

FIGURE 18. The three types of faces of ∂P_σ.

The remaining faces of P_σ are in bijective correspondence with the edges of P. Let e be an edge of P, and let b be the barycenter of e. We have constructed exactly two edges e_1 and e_2 in ∂P_σ which contain b and are not contained in e. The edge e determines a quadrilateral face of P_σ containing $e_1 \cup e_2$ and the barycenter u of the 3-cell of P. If e is contained in two distinct faces of P, then the face of P_σ determined by e has four distinct edges as in the first diagram of Figure 19. If e is contained in just one face of P, then the face of P_σ determined by e is a degenerate quadrilateral as in the second diagram of Figure 19. We have now described all the faces of P_σ. This determines P_σ. Note that every vertex of P is in a unique 3-cell of P_σ.

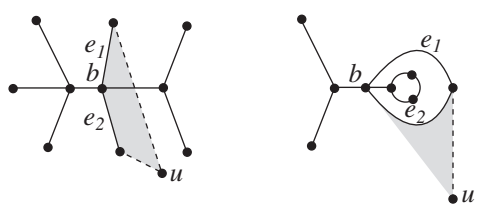

FIGURE 19. Faces of P_σ not contained in ∂P_σ.

Now that we have defined dual cap subdivisions of faceted 3-balls, we define dual cap subdivisions of more general cell complexes. Let X be a CW complex which is the union of its 3-cells, and suppose that for every 3-cell C of X there exists a faceted 3-ball P and a continuous cellular map $\varphi\colon P \to C$ such that the restriction of φ to every open cell of P is a homeomorphism. We say that a subdivision X_σ of X is a dual cap subdivision of X if for every such choice of C the cell structure on C induced from X_σ pulls back via φ to give a dual cap subdivision of P.

It is now clear how to also define a dual cap subdivision of every CW complex with dimension at most 2 such that every 2-cell contains an edge. If X is a cell complex for which we have defined a dual cap subdivision and k is a positive integer, then we let X_{σ^k} denote the k-th dual cap subdivision of X.

3.2. **Structure of 3-cells.** In this subsection we discuss the structure of the 3-cells which occur in the dual cap subdivision of a faceted 3-ball.

Let P be a regular faceted 3-ball. In Section 4 of [2] we showed that every 3-cell of P_σ is an alternating suspension. Every 3-cell of P_σ contains exactly one vertex of P, and every vertex of P is contained in exactly one 3-cell of P_σ. If v is a vertex of P with valence k, then the 3-cell of P_σ which contains v is an alternating suspension of a $2k$-gon. See Figure 20, which is the same as Figure 15 of [2]. In Figure 20 the vertex v is a vertex of P and u is the barycenter of the 3-cell of P. Figure 20 shows an alternating suspension of an octagon.

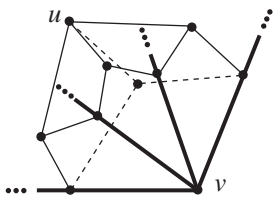

FIGURE 20. The 3-cell of P_σ which contains the vertex v of P.

Now we consider the case of a general faceted 3-ball P. Let v be a vertex of P. Let $e_1, \ldots, e_k$ be the edges of P_σ which contain v. For every $i \in \{1, \ldots, k\}$ let v_i be the vertex of e_i unequal to v. There are k corners of faces at v. Let $f_1, \ldots, f_k$ be the faces which contain these corners. Let u be the barycenter of the 3-cell of P, and let u_i be the barycenter of f_i for every $i \in \{1, \ldots, k\}$. If $u_1, \ldots, u_k$ and $v_1, \ldots, v_k$ are distinct, then just as in the previous paragraph, there is exactly one 3-cell of P_σ which contains v and this 3-cell is an alternating suspension of a $2k$-gon with cone points u and v. In general exactly one 3-cell of P_σ contains v and every 3-cell of P_σ contains exactly one vertex of P. The 3-cell of P_σ which contains v is a quotient of an alternating suspension of a $2k$-gon with cone points mapping to u and v, the identifications arising as follows. If $f_i = f_j$ for some $i, j \in \{1, \ldots, k\}$, then $u_i = u_j$, and so the edge joining u and u_i equals the edge joining u and u_j. If $v_i = v_j$ for some $i, j \in \{1, \ldots, k\}$, then the face containing u and v_i equals the face containing u and v_j. So the 3-cell of P_σ which contains v is a quotient of an alternating suspension of a $2k$-gon with cone points mapping to u and v. The quotient map performs two kinds of identifications. Edges containing the cone point which maps to u are identified if some face of P is not locally an embedded disk at v. Faces containing the cone point which maps to u are identified if some edge of P is not locally an embedded line segment at v. In every case the restriction of the quotient map to every open cell of the alternating suspension is a homeomorphism.

3.3. **Central balls.** In this subsection and the next we investigate the second dual cap subdivision of a faceted 3-ball.

Let P be a faceted 3-ball. Let u be the vertex of P_σ which is the barycenter of the 3-cell of P. Let C be a 3-cell of P_σ. Section 3.2 shows that C contains u and that C is a quotient of an alternating suspension B. One of the cone points u' of B maps to u. It easily follows from Section 3.2 that there exists a cellular homeomorphism $\theta\colon \operatorname{star}(u', B_\sigma) \to B$ such that the action of θ on the vertices of $\operatorname{star}(u', B_\sigma)$ is characterized by the property that if x is a vertex of $\operatorname{star}(u', B_\sigma)$ and if X is a cell of B for which $x \in X$, then $\theta(x) \in X$. It is now easy to see that this

assertion for B carries over to the following assertion for C. There exists a cellular homeomorphism $\psi_C\colon \operatorname{star}(u, C_\sigma) \to C$ such that the action of ψ_C on the vertices of $\operatorname{star}(u, C_\sigma)$ is characterized by the property that if x is a vertex of $\operatorname{star}(u, C_\sigma)$ and if X is a cell of C for which $x \in X$, then $\psi_C(x) \in X$. It is now easy to see that there exists a cellular homeomorphism $\psi\colon \operatorname{star}(u, P_{\sigma^2}) \to P_\sigma$ such that the action of ψ on the vertices of $\operatorname{star}(u, P_{\sigma^2})$ is characterized by the property that if x is a vertex of $\operatorname{star}(u, P_{\sigma^2})$ and if X is a cell of P_σ for which $x \in X$, then $\psi(x) \in X$. We call $\operatorname{star}(u, P_{\sigma^2})$ the **central ball** of P_{σ^2}. We have just shown that the central ball of P_{σ^2} is cellularly homeomorphic to P_σ in a way which is canonical on vertices.

3.4. **Chimneys.** Let P be a faceted 3-ball. Let u be the vertex of P_σ which is the barycenter of the 3-cell of P. Let A_1 be the star of u in the 1-skeleton of P_σ. Let $A = \operatorname{star}(A_1, P_{\sigma^2})$. We call A the **chimney assembly** for P. This subsection is devoted to investigating the structure of chimney assemblies.

Let f be a face of P, and let a be the vertex of P_σ which is the barycenter of f. Then $\operatorname{star}(a, P_{\sigma^2})$ is a subcomplex of A, which we call the f-**chimney** of A.

Let f be a face of P. Let F be a CW complex such that F is a closed disk, the interior of F is the unique open 2-cell of F and there exists a continuous cellular map $\varphi\colon F \to f$ such that the restriction of φ to every open cell of F is a homeomorphism. Given a dual cap subdivision f_σ of f, we choose a dual cap subdivision F_σ of F so that φ induces a cellular map $\varphi_\sigma\colon F_\sigma \to f_\sigma$. Let C_f be the mapping cylinder of φ_σ, viewed as a CW complex in the obvious way.

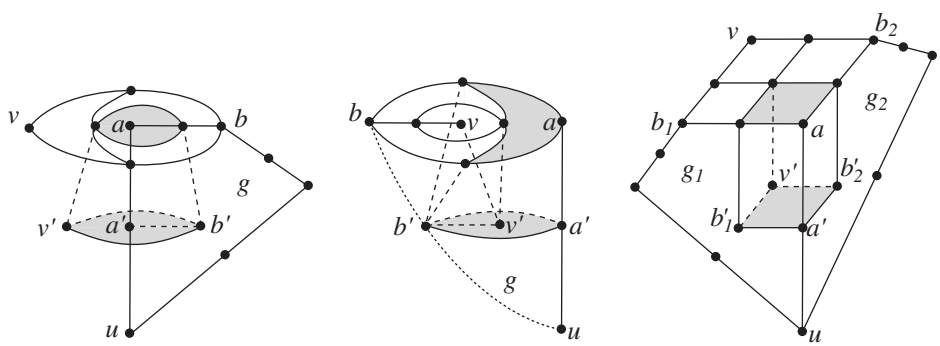

FIGURE 21. Part of P_{σ^2}.

In this and the next four paragraphs we show that C_f is cellularly homeomorphic to the f-chimney of A. Let a be the barycenter of f and let v be a vertex of f. Recall from Figure 18 and the discussion in Section 3.1 that there are three possibilities for a face of ∂P_σ. For each of the three possibilites, Figure 21 shows part of P_{σ^2}. Every vertex and edge in Figure 21 is a vertex or edge of P_{σ^2} except for the dotted arc in the second diagram which joins b, b', and u. The barycenter a of f is shown. In the first two diagrams b is the barycenter of the edge of f that contains v, and a, b, and v are the vertices of a face h of f_σ. In the third diagram b_1 and b_2 are the barycenters of the two edges of f that contain v, and a, b_1, b_2, and v are the vertices of a face h of f_σ. The dual cap subdivision of h is shown in Figure 21. The barycenter u of P and a are joined by an edge e of P_σ. Let a' be the barycenter of e in P_{σ^2}. Let the map $\psi\colon \operatorname{star}(u, P_{\sigma^2}) \to P_\sigma$ be as in Section 3.3. Section 3.3

shows that $\psi(a') = a$. Let C be the 3-cell of P_σ which contains v, and let v' be the barycenter of C in P_{σ^2}. Section 3.3 shows that $\psi(v') = v$. Let k be the face of h_σ which contains a. In each of the three diagrams in Figure 21 we have drawn in gray the face k and a face h' which will be described below. We consider separately the three possibilities for h shown in Figure 18.

We first consider the case that h has the form of the first diagram in Figure 18. Then f is a monogon. Let g be the face of P_σ which contains a, b, and u, and let b' be the barycenter of g. For clarity, two edges of g_σ are not shown. Section 3.3 shows that $\psi(b') = b$. Let h' be the face of P_{σ^2} with vertices a', b', and v'. It is easy to see in this case that k and h' are cellularly homeomorphic, $\mathrm{star}(a, P_{\sigma^2})$ is the product of a 1-simplex and the dual cap subdivision of a monogon, and so $\mathrm{star}(a, P_{\sigma^2})$ is cellularly homeomorphic to C_f.

Now suppose that h has the form of the second diagram in Figure 18. Then v has valence 1 in ∂f. As in the previous case let g be the face of P_σ which contains a, b, and u, and let b' be the barycenter of g. Section 3.3 again shows that $\psi(b') = b$. Let h' be the face of P_{σ^2} with vertices a', b, and v'. Then k is cellularly homeomorphic to a square and h' is cellularly homeomorphic to a square with two adjacent edges identified. It follows that the 3-cell of $\mathrm{star}(a, P_{\sigma^2})$ which contains v' is cellularly homeomorphic to a cube with two adjacent edges identified.

Finally, suppose h has the form of the third diagram in Figure 18. For $i \in \{1, 2\}$, let g_i be the face of P_σ which contains u and b_i and let b'_i be the vertex of P_{σ^2} which is the barycenter of g_i. For clarity two edges of $(g_1)_\sigma$ and two edges of $(g_2)_\sigma$ are omitted in the third diagram in Figure 21. Section 3.3 shows that $\psi(b'_i) = b_i$ for $i \in \{1, 2\}$. Let h' be the face of P_{σ^2} with vertices a', b'_1, b'_2 and v'. We see that ψ restricts to a cellular homeomorphism from h' to h. Then both k and h' are cellularly homeomorphic to squares and the 3-cell of $\mathrm{star}(a, P_{\sigma^2})$ which contains v' is cellularly homeomorphic to a cube.

If h has the form of the second or third diagram in Figure 18, then $\mathrm{star}(a, P_{\sigma^2})$ is a union of complexes as described in the previous two paragraphs. It easily follows that in these cases $\mathrm{star}(a, \partial P_{\sigma^2})$ is cellularly homeomorphic to F_σ, that the restriction of ψ to $\mathrm{star}(a, P_{\sigma^2}) \cap \mathrm{star}(u, P_{\sigma^2})$ is a cellular homeomorphism onto f_σ and that $\mathrm{star}(a, P_{\sigma^2})$ is cellularly homeomorphic to C_f.

So the chimney assembly A for P is the union of the central ball of P_{σ^2} and the chimneys of the faces of P. The central ball of P_{σ^2} is cellularly homeomorphic to P_σ, and the chimneys of the faces of P are mapping cylinders. Figure 22 shows the chimney assembly for a cube.

Let f be a face of P, and let C_f be the f-chimney of A. We call $f \cap C_f$ the **top** of C_f. We call the intersection of C_f with the central ball of A the **bottom** of C_f. We call faces of ∂C_f which are in neither the top nor the bottom of C_f **lateral faces**.

4. Constructing Heegaard diagrams from face-pairings

In this section we construct Heegaard diagrams from face-pairings.

4.1. **Edge pairing surfaces.** We begin by constructing a cellulated closed surface S from a face-pairing. We call S the **edge pairing surface** of the face-pairing. See the introduction, where S is defined for regular faceted 3-balls. Our more general faceted 3-balls present some complications, but we proceed in much the same way.

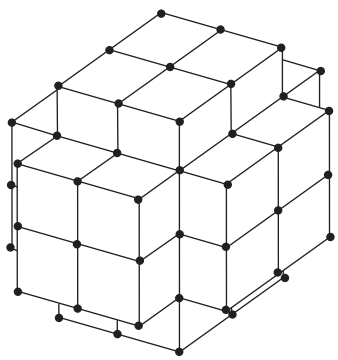

FIGURE 22. The chimney assembly for a cube.

Let P be a faceted 3-ball with orientation-reversing face-pairing ϵ. We first construct a cell complex X cellularly homeomorphic to the 1-skeleton of P. Let f and f^{-1} be two paired faces of P. Next construct a CW complex F such that F is a closed disk, the interior of F is the unique open 2-cell of F and there exists a continuous cellular map $\varphi\colon F \to f$ such that the restriction of φ to every open cell of F is a homeomorphism. There also exists a corresponding cellular map $\psi\colon F \to f^{-1}$ such that φ and ψ are related as follows. Recall that to define ϵ we construct subdivisions f_s and f_s^{-1} of f and f^{-1} in Section 2. Let t be a face of f_s. Then there exists a corresponding face t^{-1} of f_s^{-1} and a partial face-pairing map $\epsilon_t\colon t \to t^{-1}$. There also exists a subspace T of F such that the restriction of φ to T is a homeomorphism onto t. We may, and do, choose the maps φ and ψ so that if $x \in T$, then $\psi(x) = \epsilon_t(\varphi(x))$. We next construct $\partial F \times [0,1]$. We view the interval $[0,1]$ as a 1-cell, and we view $\partial F \times [0,1]$ as a 2-complex with the product cell structure. For every $x \in \partial F$ we identify $(x,0) \in \partial F \times [0,1]$ with the point of X corresponding to $\varphi(x) \in \partial f$ and we identify $(x,1) \in \partial F \times [0,1]$ with the point of X corresponding to $\psi(x) \in \partial f^{-1}$. Doing this for every pair of faces of P yields a cell complex Y whose underlying space is a closed surface. We define S to be the dual cap subdivision of Y. We say that an edge of S is **vertical** if it is either contained in X or is disjoint from X. We say that an edge of S is **diagonal** if it is not vertical. We say that an edge of S is a **meridian edge** if it is not an edge of Y. We refer to edges of Y as **nonmeridian** edges of S.

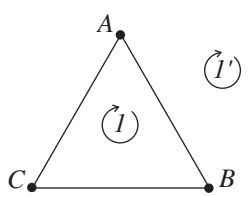

FIGURE 23. The complex P for Example 4.1.1.

Example 4.1.1. *We illustrate the above edge pairing surface construction using the simple example of the lens space $L(3,1)$. To obtain $L(3,1)$ we take a faceted 3-ball P with just two faces which are triangles as in Figure 23, where one face is at*

infinity. The orientation-reversing face-pairing map ϵ_1 maps the inner triangle to the outer triangle taking vertex A to vertex B. We set $\epsilon = \{\epsilon_1^{\pm 1}\}$. Let S be the edge pairing surface of ϵ, and let $\widetilde{A}$, $\widetilde{B}$ and $\widetilde{C}$ be the vertices of S which correspond to A, B and C. Figure 24 shows S as an annulus whose boundary components are to be identified in a straightforward way. Similarly, Figure 25 shows S as a quotient of a quadrilateral. This quadrilateral is gotten from the edge cycle of ϵ, shown in Figure 26, in a straightforward way. The meridian edges of S are drawn with thin arcs, and the nonmeridian edges of S are drawn with thick arcs. We see that S is a torus. The union of the vertical meridian edges is a simple closed curve on the torus, and the union of the diagonal meridian edges is a simple closed curve on the torus. The torus and these two curves form a Heegaard diagram for $L(3,1)$. This is a special case of Theorem 4.2.1.

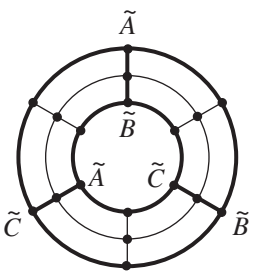

FIGURE 24. The edge pairing surface of ϵ viewed as a quotient of an annulus.

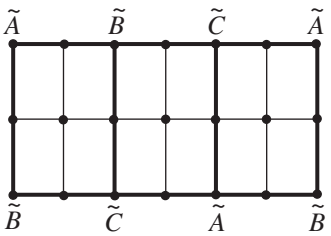

FIGURE 25. The edge pairing surface of ϵ viewed as a quotient of a quadrilateral.

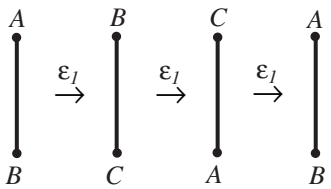

FIGURE 26. A diagram of the edge cycle of ϵ.

4.2. **Heegaard diagrams for general face-pairings.**

Theorem 4.2.1. *Let P be a faceted 3-ball with orientation-reversing face-pairing ϵ. Suppose that the cell complex $N = P/\epsilon$ is a manifold with one vertex. Let H_1 be the star of the barycenter of the 3-cell of N in the 1-skeleton of N_σ, and let $H = star(H_1, N_{\sigma^2})$. Then H is a handlebody in N such that ∂H is a Heegaard surface for N. Furthermore ∂H is cellularly homeomorphic to the edge pairing surface S of ϵ. The union of the edges of ∂H corresponding to the vertical meridian edges of S forms a basis of meridian curves for H, and the union of the edges of ∂H corresponding to the diagonal meridian edges of S forms a basis of meridian curves for the closure of the complement of H in N. So S and its two families of curves which are unions of meridian edges form a Heegaard diagram for N.*

Proof. We view N_{σ^2} as a quotient of P_{σ^2}. The preimage of H in P_{σ^2} is the chimney assembly A for P. Hence it is easy to see that H is a handlebody in N and that the closure of the complement of H in N is the star of the 1-skeleton of N in N_{σ^2}. Hence the closure of the complement of H in N is also a handlebody, and so ∂H is a Heegaard surface for N.

In this paragraph we show that ∂H is cellularly homeomorphic to S. The preimage of ∂H in P_{σ^2} is the union of all the lateral faces of the chimneys of A. Section 3.4 shows that every chimney of A is a mapping cylinder, and so the union of the lateral faces of every chimney of A is a mapping cylinder. It is now easy to see that S is defined so that S is cellularly homeomorphic to ∂H.

Let f be a face of P. The top of the f-chimney C_f of A meets the union of the lateral faces of C_f in a simple closed edge path in A. This edge path maps to a meridian curve for H, and every edge in this meridian curve corresponds to a vertical meridian edge of S. It easily follows that the union of the edges of ∂H corresponding to the vertical meridian edges of S forms a basis of meridian curves for H.

Let H' denote the closure of the complement of H in N. Suppose given an edge cycle of ϵ consisting of j distinct edges $e_1, \ldots, e_j$ of P with diagram

$$e_1 \xrightarrow{\epsilon_{f_1}} e_2 \xrightarrow{\epsilon_{f_2}} \cdots \xrightarrow{\epsilon_{f_{j-1}}} e_j \xrightarrow{\epsilon_{f_j}} e_1.$$

Let u be the vertex of P_{σ^2} which is the barycenter of the 3-cell of P, and let $\psi\colon \operatorname{star}(u, P_{\sigma^2}) \to P_\sigma$ be the cellular homeomorphism of Section 3.3. Let $e_i' = \psi^{-1}((e_i)_\sigma)$, let v_i be the vertex of e_i' such that $\psi(v_i)$ is the barycenter of e_i and let C_{f_i} be the f_i-chimney of A for every $i \in \{1, \ldots, j\}$. For every $i \in \{1, \ldots, j\}$ the chimney C_{f_i} contains two lateral faces and the chimney $C_{f_i^{-1}}$ contains two lateral faces with the following properties, where $i+1$ is taken modulo j. See Figure 27. The two lateral faces of C_{f_i} both contain an edge which contains v_i and a vertex x_i in the top of C_{f_i}, and the two lateral faces of $C_{f_i^{-1}}$ both contain an edge which contains v_{i+1} and a vertex y_i in the top of $C_{f_i^{-1}}$. Furthermore the image in ∂H of x_i equals the image in ∂H of y_i, and both the edge containing v_i and x_i and the edge containing v_{i+1} and y_i map to edges of ∂H which correspond to diagonal meridian edges of S. It is easy to see that the union of these $2j$ edges of ∂H is a closed edge path in $\partial H = \partial H'$ which bounds a subcomplex of H' which is a properly embedded closed disk. If ϵ has m edge cycles, then we obtain m such disks $D_1, \ldots, D_m$ in H'. It is easy to see that $D_1, \ldots, D_m$ are pairwise disjoint and that $H' \setminus \bigcup_{i=1}^m D_i$ has one connected component for every vertex of N and that each of these connected

components contracts to the corresponding vertex. Since N has only one vertex, it follows that $D_1, \ldots, D_m$ form a basis of meridian disks for H', and so the union of the edges of ∂H corresponding to the diagonal meridian edges of S forms a basis of meridian curves for H'.

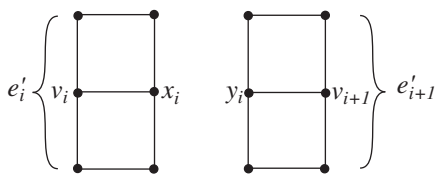

FIGURE 27. Two lateral faces of C_{f_i} and two lateral faces of $C_{f_i^{-1}}$.

This proves Theorem 4.2.1. □

4.3. **Heegaard diagrams for twisted face-pairing 3-manifolds.** In this subsection we interpret Theorem 4.2.1 for twisted face-pairing 3-manifolds.

Let P be a faceted 3-ball with orientation-reversing face-pairing ϵ, and suppose given a multiplier function for ϵ. Let Q be the associated twisted face-pairing subdivision of P, let δ be the associated twisted face-pairing on Q, and let $M = Q/\delta$ be the associated twisted face-pairing manifold. Let S be the edge pairing surface of δ.

Theorem 4.2.1 implies that S is cellularly homeomorphic to a Heegaard surface for M. We view S as a union of subspaces, one for every edge cycle of ϵ as follows. Let E be an edge cycle of ϵ. Suppose that E has length j, multiplier k and edge cycle diagram

$$e_1 \xrightarrow{\epsilon_{f_1}} e_2 \xrightarrow{\epsilon_{f_2}} \cdots \xrightarrow{\epsilon_{f_{j-1}}} e_j \xrightarrow{\epsilon_{f_j}} e_1.$$

To construct Q from P we subdivide each of the edges $e_1, \ldots, e_j$ into jk subedges. Every edge of Q gives rise to two edges of S. So the edges $e_1, \ldots, e_j$ of P give rise to subcomplexes $\widetilde{e}_1, \ldots, \widetilde{e}_j$ of S each of which is the union of $2jk$ edges of S. As in Figure 11 of [2], δ maps subedge m of e_i relative to f_i to subedge $m+1$ of e_{i+1} relative to f_{i+1} for every $i \in \{1, \ldots, j\}$ and $m \in \{1, \ldots, jk-1\}$, where $i+1$ is taken modulo j. It follows that E gives rise to a subspace C of S as shown in Figure 28. We call C an **edge cycle cylinder**. Certain arcs contained in C are not edges of S, and so they are drawn with dashes. The edges of S are drawn with two thicknesses simply to distinguish the thin meridian edges from the thick nonmeridian edges of S. In general C need not be homeomorphic to a closed annulus, but there exists a closed annulus A and a surjective continuous map $\varphi\colon A \to C$ such that the restriction of φ to the interior of A is a homeomorphism and φ maps the boundary of A to the union of the arcs drawn with dashes in Figure 28. We refer to the images under φ of the two boundary components of A as the **ends** of C. The ends of C are chosen so that the edge cycle cylinders corresponding to different ϵ-edge cycles meet only along their boundaries and their union is S. If γ is an arc in A which joins the boundary components of A, then we say that the curve $\varphi(\gamma)$ **joins the ends** of C. If γ is a simple closed curve in the interior of A which separates the boundary components of A, then we say that the curve $\varphi(\gamma)$ **separates the ends** of C. We define the **circumference** of C to be j, and we define the **height** of C to be jk. Now we see that Figure 11 of [2] essentially shows an edge cycle cylinder in

a Heegaard surface for M. The thick vertical edges in Figure 28 arise from P, and the thick diagonal edges in Figure 28 arise from P^*. Vertical edges of S are drawn vertically, and diagonal edges of S are drawn diagonally. The following theorem is now clear.

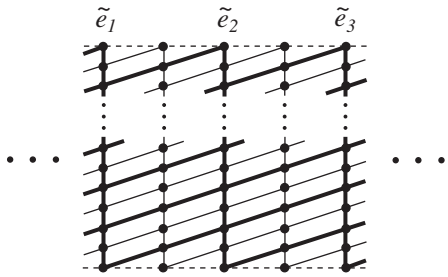

FIGURE 28. The edge cycle cylinder corresponding to the ϵ-edge cycle E.

Theorem 4.3.1. *Let P be a faceted 3-ball with orientation-reversing face-pairing ϵ, and suppose given a multiplier function for ϵ. Let δ be the associated twisted face-pairing, and let M be the associated twisted face-pairing manifold. The edge pairing surface S of δ is homeomorphic to a Heegaard surface for M. The surface S can be constructed as a union of edge cycle cylinders as in the previous paragraph. These edge cycle cylinders contain vertical meridian edges and diagonal meridian edges. The union of the vertical meridian edges of S is a basis of meridian curves for S, and the union of the diagonal meridian edges of S is a basis of meridian curves for S. Finally, S and these two families of curves form a Heegaard diagram for M.*

Example 4.3.2. *We return to Example 2.1. The model face-pairing in Example 2.1 has three edge cycles. Line 2.2 gives diagrams for them. As in Example 2.1, we choose multipliers to be 4, 1 and 1. Each of these three edge cycles gives rise to an edge cycle cylinder as in Figure 28. These three edge cycle cylinders are shown in Figure 29. They are drawn as quadrilaterals with their left sides to be identified with their right sides. The first edge cycle cylinder has circumference 1 and height 4, the second has circumference 2 and height 2 and the third has circumference 2 and height 2. The thin dotted arcs in Figure 29 indicate how the ends of the cylinders are to be identified. These identifications respect the face-pairing maps, which are also shown. After performing the required identifications we obtain a closed orientable surface S of genus 2. The union of its vertical meridian edges is a basis of meridian curves for S, and the union of its diagonal meridian edges is a basis of meridian curves for S. The result is a Heegaard diagram for our twisted face-pairing manifold.*

5. Constructing face-pairings from Heegaard diagrams

In Section 4 we construct Heegaard diagrams from face-pairings. Theorem 4.3.1 shows that every twisted face-pairing manifold has a Heegaard diagram which can be decomposed into cylinders which correspond to the edge cycles of the model face-pairing. The height of every such cylinder is a multiple of its circumference,

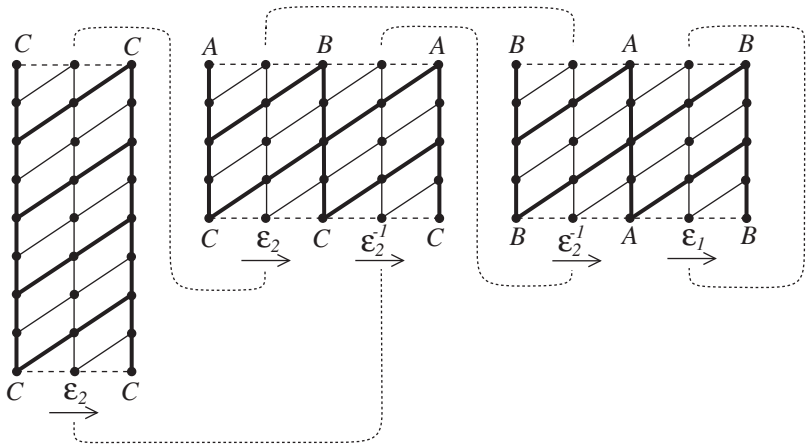

FIGURE 29. A Heegaard diagram decomposed into three edge cycle cylinders.

the multiple being the multiplier of the corresponding edge cycle. In this section we show that the decomposition of Heegaard diagrams into analogous cylinders is a general phenomenon, not one restricted to twisted face-pairing manifolds. In general the heights of the cylinders need not be multiples of their circumferences. In fact, Theorem 5.3.1 shows that the height of every such cylinder coming from a given Heegaard diagram is a multiple of its circumference if and only if the Heegaard diagram arises from a twisted face-pairing manifold as in Theorem 4.3.1. This provides a characterization of the Heegaard diagrams which we construct for twisted face-pairing manifolds.

5.1. **Generalities concerning Heegaard diagrams.** For us a Heegaard diagram is a Heegaard diagram for a closed orientable 3-manifold. It consists of an orientable closed surface S with positive genus and two bases of meridian curves for S. We assume that there exists a triangulation of S for which each of these meridian curves is piecewise linear, and we assume that these curves intersect transversely in only finitely many points. Let U be the union of the two bases of meridian curves for S. We say that our Heegaard diagram is **irreducible** if every connected component of $S \setminus U$ is homeomorphic to an open disk.

Suppose given an irreducible Heegaard diagram consisting of an orientable closed surface S and two bases of meridian curves for S. We refer to the meridian curves in one basis as **vertical meridian curves**, and we refer to the meridian curves in the other basis as **diagonal meridian curves**. The assumptions imply that the meridian curves of our Heegaard diagram determine a cell structure on S whose vertices are the intersections of the meridian curves and whose faces are the closures of the connected components of the complement in S of the union of the meridian curves. We refer to the edges of S which are contained in vertical meridian curves as **vertical (meridian) edges**, and we refer to the edges of S which are contained in diagonal meridian curves as **diagonal (meridian) edges**. It is easy to see that every vertex of S has valence 4. It is also easy to see that the edges of every face of S are alternately vertical and diagonal, and so every face of S has an even number of edges.

5.2. **Heegaard cylinders.** Suppose given an irreducible Heegaard diagram with surface S. We view S as having a cell structure as in the last paragraph. This subsection is devoted to defining subspaces of S called Heegaard cylinders.

In this paragraph we construct what we call temporary horizontal segments of S. For this we choose an orientation of S. This orientation of S determines an orientation of the boundary of every face of S. Let f be a face of S. Let v_1 be a vertex of f such that a diagonal edge e_1 of f follows v_1 (relative to f). See Figure 30, where, as usual, faces are oriented in the clockwise direction. The vertex v_1 and the edge e_1 determine a vertical edge e_2 of f which follows e_1 (relative to f) and a terminal vertex v_2 of e_2 (relative to f). We choose an open arc in the interior of f whose closure joins v_1 and v_2. We call the closure of this open arc a **temporary horizontal segment** of S. In Figure 30, e_1 is drawn with a dashed line segment, e_2 is drawn with a line segment, the rest of the boundary of f is drawn with a broken arc and the temporary horizontal segment s joining v_1 and v_2 is drawn with a dotted line segment. We choose a temporary horizontal segment for every such choice of e_1 and e_2 so that the temporary horizontal segments associated to distinct choices of e_1 and e_2 meet only at vertices of S. Figure 31 shows a complete set of temporary horizontal segments for a digon, a quadrilateral, and a hexagon, with conventions as in Figure 30.

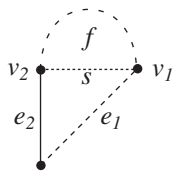

FIGURE 30. The temporary horizontal segment s of f.

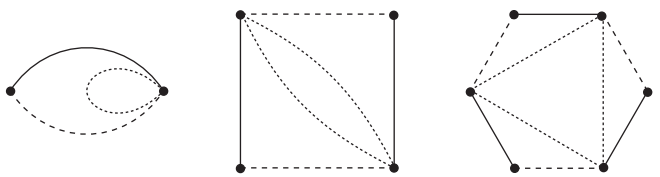

FIGURE 31. A complete set of temporary horizontal segments for a digon, a quadrilateral and a hexagon.

In this paragraph we define what it means for one temporary horizontal segment to follow another. Every vertex v of S has a neighborhood as in Figure 32. The vertex v is contained in temporary horizontal segments s_1, s_2, s_3, s_4, which need not be distinct. Rotating about v in the clockwise direction from s_1, we encounter a vertical edge, then a diagonal edge and then s_2. We say that s_2 **follows** s_1 and likewise that s_4 follows s_3. If faces are oriented in the counterclockwise direction, then we rotate about v in the counterclockwise direction. For every temporary horizontal segment s_1 of S there exists a unique temporary horizontal segment s_2 of S such that s_2 follows s_1. Furthermore, s_1 is the unique temporary horizontal segment of S such that s_2 follows s_1.

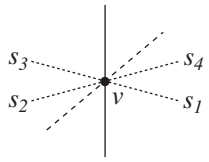

FIGURE 32. A neighborhood of a vertex v of S.

In this paragraph we use the temporary horizontal segments of S to construct annuli in S. For this let s_1 be a temporary horizontal segment of S. The previous paragraph implies that there exist temporary horizontal segments $s_2, \ldots, s_k$ such that s_{i+1} follows s_i for every $i \in \{1, \ldots, k\}$, where $i+1$ is taken modulo k. The union of $s_1, \ldots, s_k$ is a closed curve σ which intersects itself at most tangentially, not transversely. The temporary horizontal segment s_1 is contained in a face f of S, and s_1 is related to a diagonal edge e of f as in Figure 33. Across e from f is a face f' of S, and just as e is related to s_1, the edge e is related to a temporary horizontal segment s_1' in f' as in Figure 33. Just as s_1 determines the closed curve σ, the temporary horizontal segment s_1' determines a closed curve σ'. It is easy to see that σ and σ' are the boundary components of an open annulus in S which contains the interior of e.

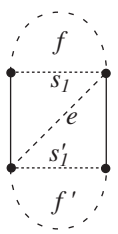

FIGURE 33. The temporary horizontal segment s_1' of f'.

A defect of the annuli constructed in the previous paragraph is that the union of their closures is not all of S. To remedy this defect, we homotop the temporary horizontal segments of S as indicated in Figure 34. More precisely, for every face f of S choose a barycenter b in the open subset of f bounded by temporary horizontal segments and join b with an arc to the initial vertex(s) (relative to f) of every diagonal edge of f so that these arcs meet only at b and they meet the temporary horizontal segments only at vertices. Then homotop (isotop except for a digon) the temporary horizontal segments of S contained in f to the union of these arcs, fixing endpoints. We refer to the image of a temporary horizontal segment under such a homotopy as a **horizontal segment**. The result of these homotopies is to enlarge the annuli of the previous paragraph so that the union of their closures is S. We refer to the closures of these enlarged annuli as **simple cylinders**. The union of the horizontal segments in a simple cylinder has two connected components, which we call the **ends** of the simple cylinder.

Suppose that $C_1, \ldots, C_k$ are simple cylinders, and suppose that C_i has ends E_i and E_i' for every $i \in \{1, \ldots, k\}$. Also suppose that the horizontal segments in E_i' equal the horizontal segments in E_{i+1} for every $i \in \{1, \ldots, k-1\}$. Then we call $C_1 \cup \cdots \cup C_k$ a **cylinder**. We define a **Heegaard cylinder** to be a cylinder which is

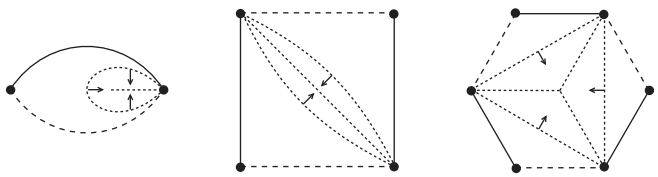

FIGURE 34. Homotoping the temporary horizontal segments in Figure 31.

maximal with respect to containment. We define the **height** of a Heegaard cylinder to be the number of simple cylinders contained in it. We define the **circumference** of a Heegaard cylinder to be the number of diagonal edges in any simple cylinder contained in the given Heegaard cylinder. The interiors of the simple cylinders of S are pairwise disjoint, and the union of the simple cylinders of S is S. It easily follows that the interiors of the Heegaard cylinders of S are pairwise disjoint, and the union of the Heegaard cylinders of S is S.

5.3. **Face-pairings for general Heegaard diagrams.**

Theorem 5.3.1. *Suppose given an irreducible Heegaard diagram D. Then there exists a faceted 3-ball P with orientation-reversing face-pairing ϵ such that $N = P/\epsilon$ is a manifold with one vertex and D is the Heegaard diagram of N described in Theorem 4.2.1. Furthermore, D is the Heegaard diagram of a twisted face-pairing manifold as described in Theorem 4.3.1 if and only if the height of every Heegaard cylinder of D is a multiple of its circumference.*

Proof. Let S be the surface of the Heegaard diagram D. We begin by defining a 1-complex K, which is a subspace of S. Recall that homotoping the temporary horizontal segments to the horizontal segments in Section 5.2 involves choosing a barycenter for every face of S. These barycenters are the vertices of K. The edges of K are dual to the diagonal edges of S. In other words, for every diagonal edge e of S there are faces f_1 and f_2 of S on either side of e, and there is an edge of K corresponding to e which joins the barycenters of f_1 and f_2.

Let V be the union of the vertical meridian curves of D. Then $S \setminus V$ is homeomorphic to the 2-sphere with $2g$ holes, where g is the genus of S. Of course, we construct K so that $K \subseteq S \setminus V$. Now it is easy to see that K is a strong deformation retract of $S \setminus V$. Figure 35 indicates how to retract $S \setminus V$ to K. In Figure 35 horizontal segments are drawn with dotted arcs, diagonal edges are drawn with dashed arcs, edges of K are drawn with thick arcs, vertical edges are drawn with medium thick arcs and retraction fibers are drawn with thin arcs and dotted arcs. It easily follows that K is cellularly homeomorphic to the 1-skeleton of a faceted 3-ball P with $2g$ faces such that a neighborhood of K in ∂P is homeomorphic to $S \setminus V$. We identify K with the 1-skeleton of P.

There exists an orientation-reversing face-pairing ϵ on P which acts on the vertices and edges of K as follows. Let e be an edge of K with vertices v_1 and v_2. By definition e is dual to a diagonal edge d of S. Let v be a vertex of this diagonal edge of S. See Figure 36, where conventions are as in Figure 35. A vertical meridian curve of D passes through v. Let d' be the diagonal edge of S incident to v across this vertical meridian curve from d. Let e' be the edge of K dual to d', and let v_1' and v_2' be the vertices of e' corresponding to the vertices v_1 and v_2 of e as in Figure 36. The vertex v determines a face f of P which contains e and a face f^{-1}

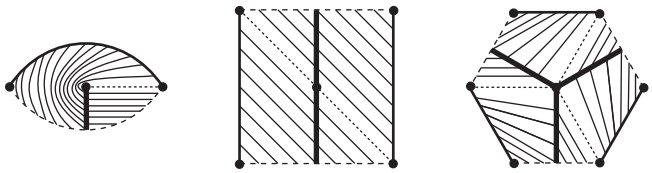

FIGURE 35. Fibers of a retraction from $S \setminus V$ to K.

which contains e'. Then the (multivalued) face-pairing map ϵ_f maps e to e' taking v_1 to v_1' and v_2 to v_2'.

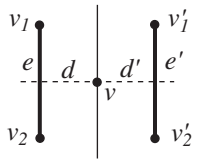

FIGURE 36. Part of S near v.

In this paragraph we show that the cell complex $N = P/\epsilon$ is a manifold with one vertex. As in the proof of the main theorem of [1], to prove that N is a manifold, it suffices to prove that the Euler characteristic of N is 0. It is clear that N has one 3-cell and g faces. So as in the proof of the main theorem of [1], to prove that N is a manifold, it suffices to prove that N has one vertex and g edges. The description of ϵ in the previous paragraph shows that the ϵ-edge cycles are in bijective correspondence with the diagonal meridian curves of D. Since D has g diagonal meridian curves, it follows that N has g edges. Just as we defined the 1-complex K with edges dual to the diagonal edges of S, it is possible to define a 1-complex K^* with edges dual to the vertical edges of S. See Figure 37, which is the same as Figure 36, except that two edges of K^* are added as thick dashed line segments. Just as the complex K is connected, so is the complex K^*. The connectivity of K^* and the description of ϵ in the previous paragraph imply that N has one vertex. Thus N is a manifold with one vertex.

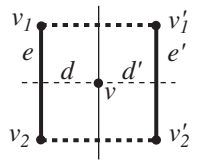

FIGURE 37. Part of S near v.

From Figure 37 it is easy to see that there exists a homeomorphism from S to the edge pairing surface S' of ϵ such that the vertical edges of S map to vertical meridian edges of S' and diagonal edges of S map to diagonal meridian edges of S'. It follows that D is the Heegaard diagram of N described in Theorem 4.2.1.

Now suppose that ϵ is a twisted face-pairing. The height of every edge cycle cylinder of ϵ's edge pairing surface is a multiple of its circumference. It is easy to

see that every Heegaard cylinder of D is a union of such edge cycle cylinders with pairwise disjoint interiors. Hence the height of every Heegaard cylinder of D is a multiple of its circumference.

Finally suppose that the height of every Heegaard cylinder of D is a multiple of its circumference. It is now easy to see that ϵ is a twisted face-pairing and that a model face-pairing can be chosen for ϵ so that the Heegaard cylinders of D are the edge cycle cylinders of ϵ's edge pairing surface.

This proves Theorem 5.3.1. □

6. Surgery descriptions for twisted face-pairing manifolds

The Heegaard diagrams of twisted face-pairing manifolds described in Theorem 4.3.1 easily yield surgery descriptions for these manifolds. This section deals with these surgery descriptions.

6.1. **Initial surgery descriptions.** Let P be a faceted 3-ball with orientation-reversing face-pairing ϵ, and suppose given a multiplier function for ϵ. Let M be the associated twisted face-pairing manifold. Theorem 4.3.1 describes a Heegaard diagram D for M. Let S be the surface of D. Let C be an edge cycle cylinder of D. Let α be a minimal union of vertical meridian edges of C which joins the ends of C. Figure 38 shows C as a quadrilateral whose left and right sides are to be identified, and α is shown as a union of vertical dotted edges. Let α' be the minimal union of diagonal meridian edges of C which joins the endpoints of α as in Figure 38. Let β be a simple closed curve in C which separates the ends of C. If the height of C equals the circumference of C, then α' is isotopic (relative endpoints) to a Dehn twist of α along β. Let τ be the appropriate Dehn twist, so that α' is isotopic (relative endpoints) to $\tau(\alpha)$. In general, if the ϵ-edge cycle corresponding to C has multiplier m, then the height of C divided by the circumference of C equals m and α' is isotopic (relative endpoints) to $\tau^m(\alpha)$ for the appropriate Dehn twist τ along β. In Figure 38, $m = 2$. This discussion essentially proves the following theorem.

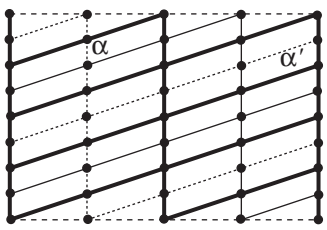

Figure 38. The curves α and α'.

Theorem 6.1.1. *Let P be a faceted 3-ball with orientation-reversing face-pairing ϵ, and suppose given a multiplier function mul for ϵ. Let $M = M(\epsilon, mul)$. Let $E_1, \ldots, E_m$ be the edge cycles of ϵ. Let D be the Heegaard diagram of M described in Theorem 4.3.1. Let S be the surface of D. Suppose that P has n pairs of faces, so that S has genus n. For every $i \in \{1, \ldots, m\}$ let C_i be the edge cycle cylinder of S corresponding to E_i. For every $i \in \{1, \ldots, m\}$ let τ_i be a Dehn twist on S along a simple closed curve in C_i which separates the ends of C_i. We choose $\tau_1, \ldots, \tau_m$ so that the directions in which they twist are consistent relative to a fixed orientation of S. Let $\tau^{mul} = \tau_1^{mul(E_1)} \circ \cdots \circ \tau_m^{mul(E_m)}$. Let $\alpha_1, \ldots, \alpha_n$ be the vertical meridian*

curves of D. Then S and $\alpha_1, \ldots, \alpha_n$ and $\tau^{mul}(\alpha_1), \ldots, \tau^{mul}(\alpha_n)$ form a Heegaard diagram for M.

Proof. The theorem follows from the previous discussion except for the matter of the directions of the Dehn twists. The previous discussion shows that every edge cycle cylinder determines a Dehn twist. It is easy to see that the twisting directions of these Dehn twists are consistent relative to a fixed orientation of S. So there are two choices for τ^{mul}. For one choice of τ^{mul} the curves $\tau^{\mathrm{mul}}(\alpha_1), \ldots, \tau^{\mathrm{mul}}(\alpha_n)$ are isotopic to the diagonal meridian curves of D, and Theorem 6.1.1 is clear. For the other choice of τ^{mul} the curves $\tau^{\mathrm{mul}}(\alpha_1), \ldots, \tau^{\mathrm{mul}}(\alpha_n)$ are isotopic to the diagonal meridian curves, not of D, but of the corresponding Heegaard diagram for the twisted face-pairing manifold M^* dual to M. Theorem 6.1.1 follows because Theorem 4.6 of [2] (together with its generalization in Section 2 if P isn't regular) shows that M^* is homeomorphic to M. □

We are now prepared for the following theorem, which shows how to obtain twisted face-pairing manifolds by Dehn surgery on framed links in S^3.

Theorem 6.1.2. *Let P be a faceted 3-ball with orientation-reversing face-pairing ϵ, and suppose given a multiplier function mul for ϵ. Let $M = M(\epsilon, mul)$. Let $E_1, \ldots, E_m$ be the edge cycles of ϵ. Let D be the Heegaard diagram of M described in Theorem 4.3.1. Let S be the surface of D. For every $i \in \{1, \ldots, m\}$ let C_i be the edge cycle cylinder of S corresponding to E_i. Suppose that P has n pairs of faces, so that S has genus n. Let $\alpha_1, \ldots, \alpha_n$ be the vertical meridian curves of D, and for every $i \in \{1, \ldots, m\}$ let β_i be a simple closed curve in C_i which separates the ends of C_i. Let H be a handlebody in S^3 with genus n such that the closure H' of $S^3 \setminus H$ is also a handlebody. Let $\gamma_1, \ldots, \gamma_n$ and $\gamma'_1, \ldots, \gamma'_n$ be curves in $\partial H = \partial H'$ such that the curves $\gamma_1, \ldots, \gamma_n$ bound a basis of meridian disks for H, the curves $\gamma'_1, \ldots, \gamma'_n$ bound a basis of meridian disks for H', the intersection $\gamma_i \cap \gamma'_i$ consists of one point for $i \in \{1, \ldots, n\}$ and $\gamma_i \cap \gamma'_j = \emptyset$ for $i \neq j$. Let $\varphi\colon S \to \partial H$ be a homeomorphism such that $\varphi(\alpha_i) = \gamma_i$ for every $i \in \{1, \ldots, n\}$. Let $A_1, \ldots, A_m$ be pairwise disjoint closed annuli in H such that for every $i \in \{1, \ldots, m\}$ one boundary component of A_i is $\varphi(\beta_i) = A_i \cap \partial H$, and let δ_i be the boundary component of A_i other than $\varphi(\beta_i)$ for every $i \in \{1, \ldots, m\}$. We obtain a link L in S^3 by taking $L = \gamma_1 \cup \ldots \cup \gamma_n \cup \delta_1 \cup \ldots \cup \delta_m$. We define a framing of L as follows. The components $\gamma_1, \ldots, \gamma_n$ have framing 0. For every $i \in \{1, \ldots, m\}$ the component δ_i has framing $lk(\delta_i, \varphi(\beta_i)) \pm mul(E_i)^{-1}$, where $lk(\delta_i, \varphi(\beta_i))$ is the linking number of δ_i and $\varphi(\beta_i)$ after they are compatibly oriented and the sign is either $+$ for every $i \in \{1, \ldots, m\}$ or $-$ for every $i \in \{1, \ldots, m\}$. Then the manifold obtained by Dehn surgery on this framed link L is homeomorphic to M.*

Proof. The surface ∂H and the curves $\gamma_1, \ldots, \gamma_n$ and $\gamma'_1, \ldots, \gamma'_n$ form a Heegaard diagram for S^3. By performing Dehn surgery on $\gamma_1, \ldots, \gamma_n$, each with framing 0, we obtain a connected sum of n copies of $S^2 \times S^1$, which has a Heegaard diagram consisting of the surface ∂H, the curves $\gamma_1, \ldots, \gamma_n$ and the curves $\gamma_1, \ldots, \gamma_n$. (The bases of meridian curves are equal.) For every $i \in \{1, \ldots, m\}$ let τ_i be a Dehn twist on ∂H along $\varphi(\beta_i)$, choosing $\tau_1, \ldots, \tau_m$ so that the directions in which they twist are consistent relative to a fixed orientation of ∂H. Set $\tau^{\mathrm{mul}} = \tau_1^{\mathrm{mul}(E_1)} \circ \cdots \circ \tau_m^{\mathrm{mul}(E_m)}$. Theorem 6.1.1 easily implies that M has a Heegaard diagram consisting of the surface ∂H, the curves $\gamma_1, \ldots, \gamma_n$ and the curves $\tau^{\mathrm{mul}}(\gamma_1), \ldots, \tau^{\mathrm{mul}}(\gamma_n)$. The fact that M is obtained by Dehn surgery on $\gamma_1, \ldots, \gamma_n$ and $\delta_1, \ldots, \delta_m$ now easily follows

from a standard argument which appears, for example, in the proof of the Dehn-Lickorish Theorem on page 84 of [6]. It only remains to determine the framings of $\delta_1, \ldots, \delta_m$.

We determine the framings of $\delta_1, \ldots, \delta_m$ in this paragraph. Let $i \in \{1, \ldots, m\}$. Let T be a solid torus regular neighborhood of δ_i such that $\varphi(\beta_i) \subseteq \partial T$. Let $\alpha \subseteq \partial T$ be the boundary of a meridian disk of T. The curve α and part of $\varphi(\beta_i)$ are shown in part a) of Figure 39. Using our usual orientation convention for figures as in Figure 38, our Dehn twist takes α to a curve γ as shown in part b) of Figure 39. Let $m = \mathrm{mul}(E_i)$. It is easy to see that γ is homologous in ∂T to $\alpha - m\varphi(\beta_i) = (1 - m\mathrm{lk}(\delta_i, \varphi(\beta_i)))\,\alpha - m\ell_i$, where $\ell_i = \varphi(\beta_i) - \mathrm{lk}(\delta_i, \varphi(\beta_i))\alpha$ is parallel to δ_i and hence is a longitude for T. Thus the framing of δ_i is $\mathrm{lk}(\delta_i, \varphi(\beta_i)) - 1/m$. If our Dehn twist is in the opposite direction, then the framing of δ_i is $\mathrm{lk}(\delta_i, \varphi(\beta_i)) + 1/m$.

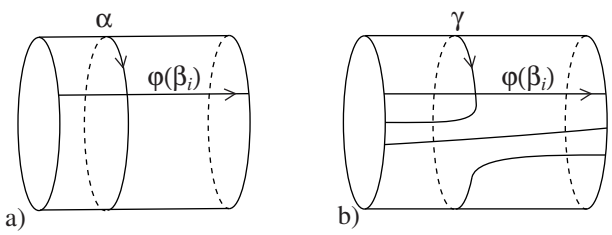

FIGURE 39. Determining the framing of δ_i.

This proves Theorem 6.1.2. □

6.2. **The corridor construction.** Theorem 6.1.2 describes a framed link L in S^3 such that Dehn surgery on L obtains a given twisted face-pairing manifold. The goal of this subsection is to make the construction of such links L algorithmic and simple. We call the method which we use the corridor construction.

Let P be a faceted 3-ball, and let ϵ be an orientation-reversing face-pairing on P. In this paragraph we construct corridors between the paired faces of P. Let f be a face of P. The face f is paired with the face f^{-1}. Let c be a corner of f at the vertex v of f, and suppose that ϵ_f takes c to the corner c' of f^{-1} at the vertex v' of f^{-1}. Let γ be an edge path arc in P with endpoints v and v'. See the left part of Figure 40, where f and f^{-1} are triangles, γ is drawn with thick line segments and the corners c and c' are indicated with dotted edges. From ∂P we construct a new cell complex with underlying space the 2-sphere as follows. We choose an arbitrarily small neighborhood of γ in ∂P and modify the cell structure of ∂P only in this neighborhood as indicated in Figure 40. The right part of Figure 40 shows the new cell complex. We refer to this modification of ∂P as **constructing a corridor** between f and f^{-1}. In a straightforward way we continue to successively construct corridors between all the paired faces of P. We call the resulting cell complex C a **corridor complex** for ϵ. Every face of C is in some sense the union of two paired faces of P and a corridor.

Again let P be a faceted 3-ball, and let ϵ be an orientation-reversing face-pairing on P. In this paragraph we describe a planar diagram D of a link L in S^3. Let C be a corridor complex for ϵ. We view the underlying space of C as the one-point compactification $\mathbf{R}^2 \cup \{\infty\}$ of $\mathbf{R}^2$, where the point ∞ lies in the interior of some face of C. The diagram D lies in $C \setminus \{\infty\}$. Let g be a face of C. We

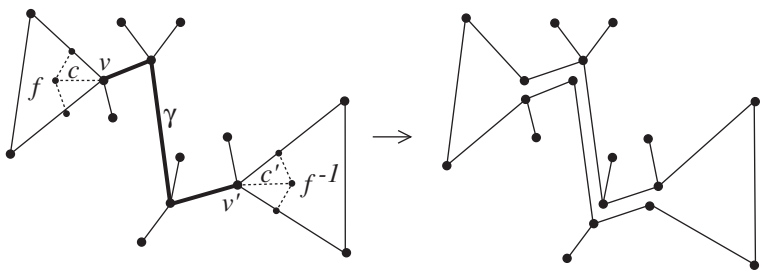

FIGURE 40. Constructing a corridor between f and f^{-1}.

next describe the part of D which lies in g. One component of L has a projection α in the interior of $g \setminus \{\infty\}$ with no self-crossings; it is unknotted. We call this component of L a **face component** of L. To describe the rest of D which lies in g, we construct a continuous map $\varphi\colon C \to \partial P$ (which is independent of g) such that 1) φ maps vertices to vertices in the canonical way, 2) the restriction of φ to every edge of C is a homeomorphism onto the canonically corresponding edge of P and 3) the restriction of φ to the inverse image of the interior of every face of P is a homeomorphism. The face g of C corresponds to two paired faces f and f^{-1} of P. Let c be an edge cone of f at an edge e (as defined in the fifth paragraph of Section 2). The face-pairing ϵ pairs c with an edge cone c' of f^{-1} at an edge e'. Then part of one component of L has a projection β in $g \setminus \{\infty\}$ such that 1) only the endpoints of β lie in an edge of g, 2) $\varphi(\beta)$ begins at the barycenter of e, 3) then an initial segment of $\varphi(\beta)$ lies in c, 4) then β crosses under α, 5) then β crosses over α, 6) then a terminal segment of $\varphi(\beta)$ lies in c' and 7) finally $\varphi(\beta)$ ends at the barycenter of e'. The corridor complex C is constructed so that we may, and do, choose the projections β for a fixed g (and f) and varying c to have no self-crossings and no crossings with each other. Constructing such projections for every face g of C obtains D. The components of L other than the face components are in bijective correspondence with the edge cycles of ϵ. We call these components of L **edge components**. We call D a **corridor complex link diagram** for ϵ. We call L a **corridor complex link** for ϵ.

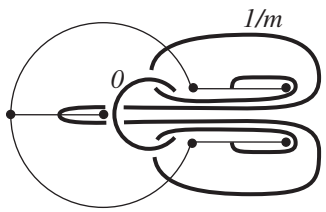

FIGURE 41. A framed corridor complex link diagram for Example 2.3.

Example 6.2.1. *We return to the model face-pairing in Example 2.3. A corridor complex for it appears in Figure 41, drawn with thin arcs. A framed corridor complex link diagram for it also appears in Figure 41, drawn with thick arcs. The model face-pairing has only one edge cycle, and we let it have multiplier m. Theorem 6.2.2 states that the associated twisted face-pairing manifold M is obtained by*

Dehn surgery on the framed link in Figure 41. It is easy to see that the framed link in Figure 41 is isotopic to a link consisting of two unlinked circles, one with framing 0 and one with framing $1/m$*. As in Proposition 14.4 of* [6]*, Dehn surgery on a circle in* S^3 *with framing 0 gives* $S^2 \times S^1$*, and as in Proposition 14.6 of* [6]*, Dehn surgery on a circle in* S^3 *with framing* $1/m$ *gives* S^3*. Thus* M *is the connected sum of* $S^2 \times S^1$ *and* S^3*. In other words,* M *is* $S^2 \times S^1$ *for every choice of the multiplier* m*.*

Theorem 6.2.2. *Let* P *be a faceted 3-ball with orientation-reversing face-pairing* ϵ*, and suppose given a multiplier function mul for* ϵ*. Let* $M = M(\epsilon, mul)$*. Let* $E_1, \ldots, E_m$ *be the edge cycles of* ϵ*. Let* D *be a corridor complex link diagram for* ϵ*. Let* L *be a link in* S^3 *with diagram* D*. We define a framing of* L *as follows. Every face component of* L *has framing 0. The edge component of* L *corresponding to* E_i *has framing* $mul(E_i)^{-1}$ *plus its blackboard framing relative to* D *for every* $i \in \{1, \ldots, m\}$*. Then the manifold obtained by Dehn surgery on the framed link* L *is homeomorphic to* M*.*

Proof. Let C be the corridor complex for ϵ from which D is constructed. As in the construction of D, we view the underlying space of C as the one-point compactification $\mathbf{R}^2 \cup \{\infty\}$ of $\mathbf{R}^2$, where the point ∞ lies in the interior of some face of C. We choose standard coordinates x, y and z for $\mathbf{R}^3$, and we identify $C \setminus \{\infty\}$ with the xy-plane in $\mathbf{R}^3$. We choose a closed standard metric ball in $\mathbf{R}^3$ centered at the origin so large that it contains every edge of C in its interior. Let X be the solid hemisphere consisting of all points of this ball on and below the xy-plane.

In this paragraph we construct a handlebody in $\mathbf{R}^3$ by attaching handles to X. Let f and f^{-1} be two paired faces of P. Let g be the face of C corresponding to f and f^{-1}. If $\infty \notin g$, then $g \subseteq \partial X$. If $\infty \in g$, then $g \cap \partial X$ has nonempty interior and is the complement in g of a neighborhood of ∞. We attach a standard handle to $g \cap X$. This handle is embedded in $\mathbf{R}^3$ so that its vertical projection to the xy-plane lies both in X and in the interior of g. Figure 42 gives a view from above of g and the handle attached to g, where both f and f^{-1} are squares joined by a simple corridor. Figure 43 gives another view of this handle. For every two paired faces of P we attach a handle to X in this way. We denote the result by H. It is clear that H is a handlebody and that the closure of the complement of H in S^3 is also a handlebody.

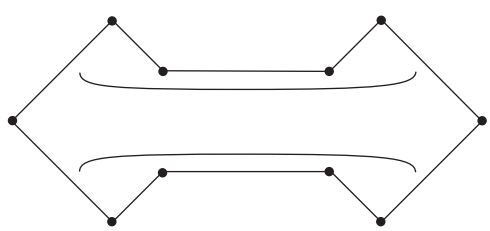

FIGURE 42. Top view of the handle attached to g.

We next construct simple closed curves in ∂H as follows. First choose a barycenter for every edge of C. Again let f and f^{-1} be two paired faces of P, and let g be the corresponding face of C. Just as in the construction of D, construct curves in ∂H which lie in and above g; these curves cross the handle and they join barycenters of edges of g which correspond to edges of f and barycenters of edges of g

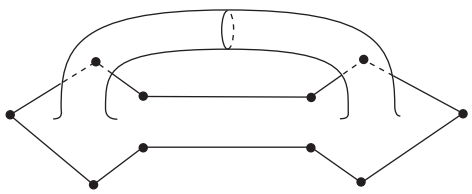

FIGURE 43. Another view of the handle attached to g.

which correspond to edges of f^{-1}. For every corridor edge e of g construct an arc in g in the obvious way which joins the barycenter of e and the barycenter of the edge of g across the corridor from e. We construct all these curves so that only their endpoints lie in edges of g and they are pairwise disjoint except possibly at endpoints. Finally, construct a meridian curve for the handle of H attached to g such that this meridian curve meets each of the curves which cross the handle exactly once. Figure 44 shows a top view of g and the handle of H attached to g with the curves just constructed drawn with thick solid and dashed arcs. Doing this for every two paired faces of P, we obtain two families of simple closed curves in ∂H. The curves $\gamma_1, \ldots, \gamma_n$ in one family are the meridian curves of the handles of H. The curves $\delta_1, \ldots, \delta_m$ in the other family correspond canonically to the edge cycles of ϵ.

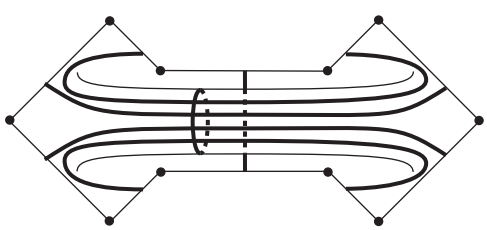

FIGURE 44. Constructing curves in the part of ∂H which project vertically to g.

Let S be the surface which appears in Theorem 6.1.2; S is the edge pairing surface of ϵ. Let the curves $\alpha_1, \ldots, \alpha_n$ and $\beta_1, \ldots, \beta_m$ be as in Theorem 6.1.2. It is easy to see that the curves $\gamma_1, \ldots, \gamma_n$ and $\delta_1, \ldots, \delta_m$ can be indexed so that there exists a homeomorphism $\varphi\colon S \to \partial H$ such that $\varphi(\alpha_i) = \gamma_i$ and $\varphi(\beta_j) = \delta_j$ for every $i \in \{1, \ldots, n\}$ and $j \in \{1, \ldots, m\}$. Theorem 6.1.2 produces a framed link L in S^3 such that the manifold obtained by Dehn surgery on L is homeomorphic to M. Finally, it is clear that D is a diagram of L and that the framings are as claimed.

This proves Theorem 6.2.2. □

7. EXAMPLES

In this section we present some examples in which we use Theorem 6.2.2 to identify some twisted face-pairing manifolds. We have already given such an example in Example 6.2.1, where we constructed a framed link in S^3 for the model face-pairing in Example 2.3. Using this we showed that the twisted face-pairing manifolds in Example 2.3 are all homeomorphic to $S^2 \times S^1$.

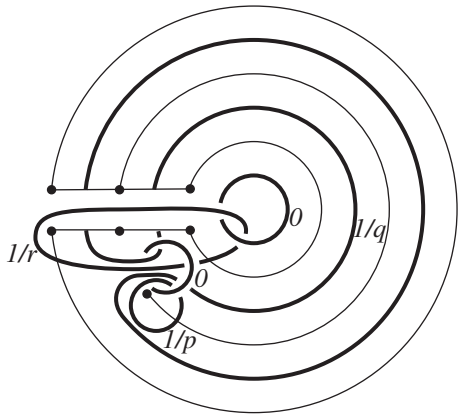

FIGURE 45. The corridor complex and framed link diagram for Example 2.1.

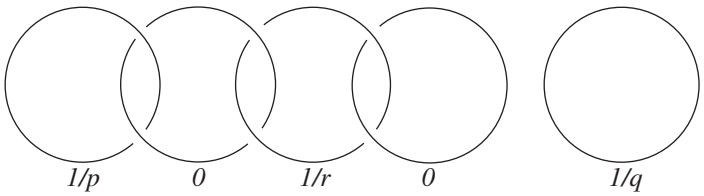

FIGURE 46. A simpler framed link.

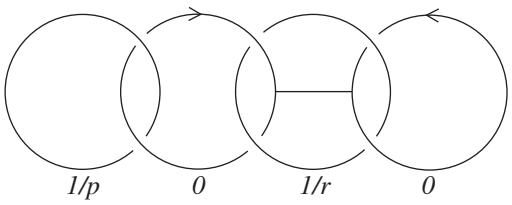

FIGURE 47. Preparing for a Kirby move of type 2.

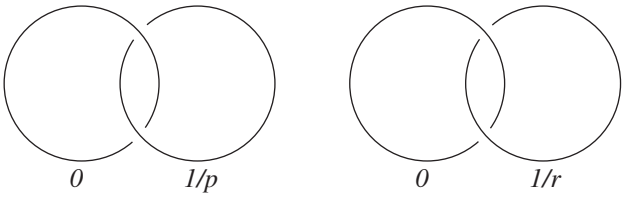

FIGURE 48. A simpler framed link.

Example 7.1. *We return to the model face-pairing in Example 2.1. We choose multipliers of the edge cycles in line 2.2 to be p, q, and r, in order. A corridor complex for Example 2.1 appears in Figure 45, drawn with thin arcs. A framed link diagram for it also appears in Figure 45, drawn with thick arcs. Theorem 6.2.2 states that the associated twisted face-pairing manifold M is obtained by Dehn surgery on*

the framed link in Figure 45. It is easy to see that the framed link in Figure 45 is isotopic to the framed link in Figure 46. The component of the link in Figure 46 with framing $1/q$ *corresponds to a connected summand of* M*. But, as in Example 6.2.1, this connected summand is* S^3*. So we delete the component of the link in Figure 46 with framing* $1/q$*. We modify the component of the link in Figure 46 with framing 0 which links the components with framings* $1/p$ *and* $1/r$ *by means of a Kirby move of type 2. For this we orient the components with framing 0 and connect them with an arc as shown in Figure 47. The result is a link isotopic to the one in Figure 48. It easily follows from Proposition 17.3 of* [6] *that* M *is a connected sum of the lens space* $L(p,-1) = L(p,1)$ *and the lens space* $L(r,-1) = L(r,1)$*.*

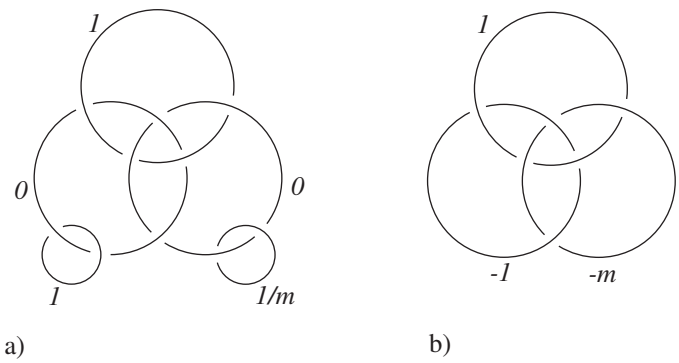

FIGURE 49. Two framed links for Example 7.2.

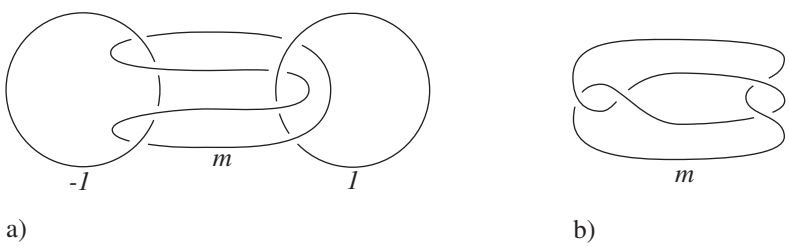

FIGURE 50. Two more framed links for Example 7.2.

Example 7.2. *We return to the model face-pairing which we described at the beginning of the introduction. We choose multipliers* $m_1 = 1$*,* $m_2 = 1$*, and* $m_3 = m$*. A corridor complex for this example appears in Figure 6, drawn with thin arcs, and a framed link diagram for it also appears in Figure 6, drawn with thick arcs. It is easy to see that the part of the link in Figure 6 which is the union of the components with framing 0 and the component which in the diagram crosses both components with framing 0 is isotopic to the Borromean rings. So the framed link in Figure 6 is isotopic to the link in part a) of Figure 49. We simplify the framed link in part a) of Figure 49 using Kirby calculus by performing twist moves, which are discussed in Sections 16.4, 16.5 and 19.4 of* [6] *under the name Fenn-Rourke moves. Twisting* $-m$ *times along the component with framing* $1/m$*, twisting* -1 *times along the*

similar component with framing 1, and deleting resulting components with framing ∞ yields the link in part b) of Figure 49. Because the link in part b) of Figure 49 is amphicheiral we may, and do, multiply every framing by -1. We isotop the result to the framed link in part a) of Figure 50. Now we perform twist moves on the link in part a) of Figure 50. We twist 1 time along the component with framing -1, twist -1 times along the component with framing 1, and delete resulting components with framing ∞. The result is shown in part b) of Figure 50. This is the figure eight knot with framing m. If $m = 1$, then M is the Brieskorn homology sphere $\Sigma(2,3,7)$, which has the geometry of the universal cover of $PSL(2,\mathbf{R})$. According to Theorem 4.7 of [7]*, M is hyperbolic if $m \geq 5$.*

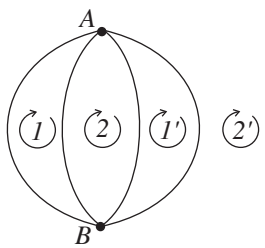

FIGURE 51. The complex P for Example 7.3.

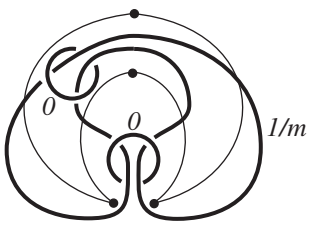

FIGURE 52. A corridor complex and framed link diagram for Example 7.3.

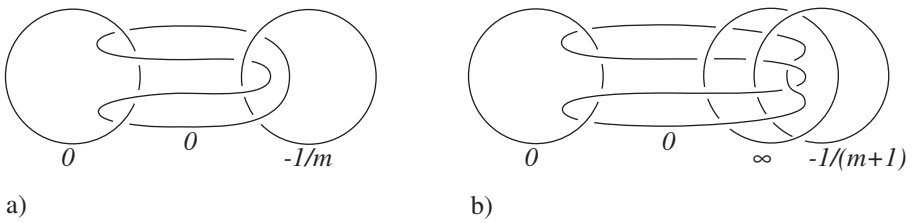

FIGURE 53. Two framed links for Example 7.3.

Example 7.3. *This example is closely related to the previous one. The model faceted 3-ball for this example is gotten from the faceted 3-ball given in Figure 1 by collapsing the edge AB to a point and collapsing the edge CD to a point. The result is the faceted 3-ball P given in Figure 51. Because the edges AB and CD in Figure 1*

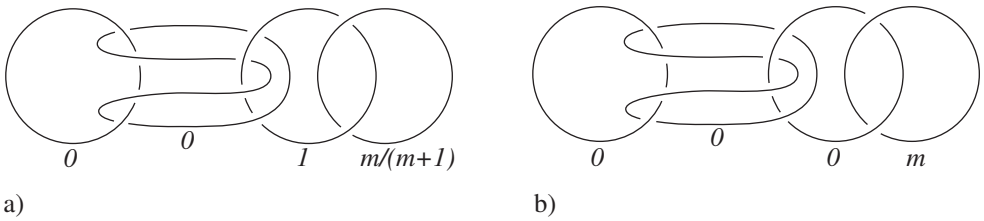

FIGURE 54. Two more framed links for Example 7.3.

are both fixed by the model face-pairing of Example 7.2, the model face-pairing of Example 7.2 induces a model face-pairing ϵ on P. The face-pairing ϵ pairs the faces of P as indicated in Figure 51, and the face-pairing maps of ϵ fix the vertices A and B. The model face-pairing ϵ has one edge cycle. This edge cycle has length 4 and corresponds to the edge cycle of length 4 in Example 7.2. We let this edge cycle of ϵ have multiplier m. A corridor complex for ϵ appears in Figure 52, drawn with thin arcs, and a framed link diagram for it also appears in Figure 52, drawn with thick arcs. This link is the Borromean rings. As in Example 7.2 we may, and do, multiply the framings by -1 and we isotop the link in Figure 52 to obtain the framed link in part a) of Figure 53. Now we perform a twist move by twisting -1 times along the component with framing $-1/m$ and we introduce a component with framing ∞ to obtain the framed link in part b) of Figure 53. Next we twist 1 time along the component with framing ∞ to obtain the link in part a) of Figure 54. Finally, we twist -1 times along the component with framing $m/(m+1)$ to obtain the link in part b) of Figure 54. The link in part b) of Figure 54 is a special case of the link at the top of Figure 12 on page 146 of [5]*. It easily follows that M is the Seifert fibered manifold $\langle Oo1|0;(m,1)\rangle$ in the notation of* [5]*. This means that M is orientable with an orientable base surface of genus 1, that the Euler number of M is 0 and that M has one exceptional fiber of type $(m,1)$. When $m=1$, the manifold M is the Heisenberg manifold, the prototype for Nil geometry.*

REFERENCES

[1] J. W. Cannon, W. J. Floyd, and W. R. Parry, *Introduction to twisted face-pairings*, Math. Res. Lett. **7** (2000), 477–491.

[2] J. W. Cannon, W. J. Floyd, and W. R. Parry, *Twisted face-pairing 3-manifolds*, preprint.

[3] J. W. Cannon, W. J. Floyd, and W. R. Parry, *Ample twisted face-pairing 3-manifolds*, preprint.

[4] J. W. Cannon, W. J. Floyd, and W. R. Parry, *A survey of twisted face-pairing 3-manifolds*, in preparation.

[5] J. M. Montesinos, *Classical Tesselations and Three-Manifolds*, Springer-Verlag, New York, 1987.

[6] V. V. Prasolov and A. B. Sossinsky, *Knots, Links, Braids and 3-Manifolds*, Amer. Math. Soc., Providence, 1997.

[7] W. P. Thurston, *The Geometry and Topology of 3-Manifolds*, Princeton lecture notes, http://www.msri.org/gt3m, 1979.

Department of Mathematics, Brigham Young University, Provo, UT 84602, U.S.A.
E-mail address: cannon@math.byu.edu

Department of Mathematics, Virginia Tech, Blacksburg, VA 24061, U.S.A.
E-mail address: floyd@math.vt.edu
URL: http://www.math.vt.edu/people/floyd

Department of Mathematics, Eastern Michigan University, Ypsilanti, MI 48197, U.S.A.
E-mail address: walter.parry@emich.edu